Seasonal variability of the boundary circulation, water masses and oxygen content in the coastal upwelling region of the eastern tropical North Atlantic

Master's Thesis

in the program **Climate Physics - Physical Oceanography and Meteorology** (M.Sc)
Faculty of Mathematics and Natural Sciences
Kiel University

Author:
Thilo Klenz
Matriculation number: 1005607

Supervisor: Prof. Dr. Peter Brandt
Second reviewer: Dr. Marcus Dengler

Kiel, December 2016

GEOMAR
Helmholtz Centre for Ocean Research Kiel

C A U
Christian-Albrechts-Universität zu Kiel

Abstract

The seasonal variability of the boundary circulation, water masses and oxygen content in the climatically and socio-economically important coastal upwelling region of the eastern tropical North Atlantic ocean is analysed. Main basis for analysis is an extensive data set consisting of nine research cruises conducted off the coast of Mauritania between the years 2005-2016.

Observations show enhanced northward flow in the upper central water layer within the poleward undercurrent and surface Mauritania current after upwelling-favorable wind stress has seized, while during the upwelling season flow over the shelf is predominantly southward and the undercurrent is weakened. Northward transports during the non-upwelling season are enhanced by a factor of three, with maximum transports during one summer cruise of $2.1Sv$. The lower central water layer is characterised by weak, southward flow year-round. The variability of the boundary circulation in the upper layers can to a large extent be explained by the seasonally varying cyclonic wind stress curl that dominates the near-coastal region year-round. Mesoscale variability in the form of eddies drives variability on shorter timescales.

Water mass analysis within the central water stratum shows that waters of South Atlantic origin transported in the boundary currents act to renew the waters of the upper central water layer during times of enhanced flow. A water mass transition at the boundary between upper and lower central waters was observed during all cruises and a mixture consisting of North and South Atlantic central waters dominates the lower layer. Seasonal variability in this layer is less pronounced, but a possible northerly ventilation pathway for this layer is apparent in the observations.

Despite the seasonal renewal of southern water masses a pronounced shallow oxygen minimum was observed around 100m water depth during the summer cruises. Lowest oxygen concentrations below $40\mu molkg^{-1}$ were observed over large parts of the study region during one summer cruise, caused by prolonged primary productivity in the surface layer and remineralization below. Enhanced diapycnal and isopycnal oxygen supply are likely the reason for higher oxygen concentrations in the range of the shallow oxygen minimum observed during the winter cruises.

Zusammenfassung

Die saisonale Variabilität der Randstromzirkulation, Wassermassen und des Sauerstoffgehalts des klimatisch und sozio-ökonomisch wichtigen Küstenauftriebsgebiets im topischen Ostatlantik wird untersucht. Grundlage für diese Untersuchungen ist ein umfassender Datensatz bestehend aus neun Forschungsfahrten, die zwischen den Jahren 2005-2016 vor der Küste Mauretaniens durchgeführt wurden.

Beobachtungen zeigen erhöhte nordwärtige Strömungen im oberen Zentralwasser im Zusammenhang mit dem polwärtigen Unterstrom und dem Mauritanienstrom an der Oberfläche nach der Hauptauftriebszeit. Während Zeiten des Küstenauftriebs ist der Strom über dem kontinentalen Schelf südwärtig und der Unterstrom geschwächt. Im Vergleich zur Auftriebszeit sind die nordwärtigen Transporte um einen Faktor drei erhöht und maximale nordwärtige Transporte von $2.1 Sv$ wurden während einer Sommerfahrt beobachtet. Im unteren Zentralwasser dominiert eine schwach südwärtige Strömung. Die Variabilität der Strömungen im oberen Zentralwasser kann zum Großteil durch die saisonale Variabilität des zyklonalen Wind Stress Curls erklärt werden, welcher im küstennahen Gebiet ganzjährig dominiert. Mesoskalige Variabilität in der Form von Wirbeln führt zudem zu Variabilität auf kürzeren Zeitskalen.

Eine Wassermassenanalyse in der Zentralwasserschicht zeigt, dass während Zeiten erhöhter Randstromzirkulation Zentralwassermassen südatlantischen Ursprungs die Wassermassen der oberen Zentralwasserschicht erneuern. Ein Wassermassenübergang an der Grenze zwischen oberem und unterem Zentralwasser konnte während aller Forschungsfahrten beobachtet werden, worunter ein Wassermassengemisch aus nord- und südatlatinschem Zentralwasser dominiert. Die saisonale Varibilität in dieser Schicht ist deutlich geringer ausgeprägt, allerdings konnte ein möglicher nördlicher Ventilationspfad in den Beobachtungen ausgemacht werden.

Trotz des saisonalen Eintrags südlicher Wassermassen wurde hauptsächlich während der Sommerfahrten ein ausgeprägtes flaches Sauerstoffminimum in etwa 100m Wassertiefe beobachtet. Die tiefsten gemessenen Sauerstoffkonzentrationen lagen dabei bei unter $40 \mu mol kg^{-1}$ über weite Teile des Beobachtungsgebiets während einer der Sommerfahrten. Der Grund für diese niedrigen Sauerstoffwerte nahe der Oberfläche steht höchstwahrscheinlich in Verbindung mit anhaltender biologischer Produktivität in den oberflächennahen Schichten und Remineralisierung darunter. Erhöhte diapyknische und isopyknische Sauerstoffflüsse führen vermutlich zu höheren Sauerstoffkonzentrationen im Bereich des flachen Sauerstoffminimums während der Winterfahrten.

Contents

Abstract i

Zusammenfassung ii

1 Introduction 1

2 Data and Methods 7

2.1 Shipboard Measurements 7

2.2 Climatological Hydrographic Data 9

2.3 Oxygen Units 10

2.4 Water Mass Analysis 10

2.5 Satellite Products 12

2.5.1 Wind Products 12

2.5.2 Sea Surface Temperature 13

2.5.3 Chlorophyll-A Concentrations 13

2.5.4 Geostrophic Surface Velocities 14

2.6 Seasonal Cycle 14

3 Oceanic Response to Seasonal Atmospheric Forcing 15

4 Results 20

4.1 Boundary Circulation 20

4.2 Hydrography and Water Mass Characteristics 27

4.3 Oxygen Distribution 35

4.4 Meridional Penetration of Water Mass Characteristics 41

5 Large-Scale Circulation from Sverdrup Dynamics 44

6 Discussion 46

7 Conclusion and Outlook 53

References 55

Acknowledgements 61

Erklärung 62

1 Introduction

The large scale circulation of the eastern tropical North Atlantic (ETNA) is determined by the southern and eastern limbs of the anticyclonic, winddriven circulation of the subtropical gyre. The Canary Current (CC), transporting oxygen-rich, relatively high salinity waters subducted in the subtropics at the eastern flank of the gyre, diverges from the West African coast at around 20°N. The North Equatorial Current (NEC) forms the westward flowing extension of the CC and the southern circulation arm of the subtropical gyre. These equator- and westward currents form the northern boundary of a shadow zone in the southern ETNA that was first predicted through a relatively simple model of the ventilated thermocline by *Luyten et al.* [1983]. The shadow zone is characterized by a weak mean circulation and hence weak ventilation. Exchange across the boundary is limited to eddies and submesoscale filaments (*Zenk et al.* [1991]). It is in this shadow zone where the oxygen minimum zone (OMZ) of the tropical North Atlantic is found.

The global oceanic oxygen distribution is generally characterized by slightly supersaturated oxygen concentrations in the surface layer and enhanced oxygen concentrations at depth. Regions of low oxygen concentrations, OMZs, at intermediate to shallow depths are a prominent feature in the eastern parts of the Pacific and Atlantic oceans as well as the northern Indian ocean (*Karstensen et al.* [2008]; *Stramma et al.* [2008b]; *Brandt et al.* [2015]). Oxygen concentrations in the North Atlantic OMZ (naOMZ) are considered *hypoxic*, with minimum oxygen concentrations between $20-40 \mu molkg^{-1}$ (*Karstensen et al.* [2008]). Two oxygen minima can be distinguished in the naOMZ. A deep minimum that is usually referred to when talking about the naOMZ is centered around 400m water depth, with minimum oxygen concentrations around 20°W, 10°N (*Fischer et al.* [2013]; *Brandt et al.* [2015]). A secondary, shallower minimum, generally found around 100m water depth, is henceforth referred to as the shallow oxygen minimum. Its minimum oxygen concentrations are much more variable below the mixed-layer and above 200m water depth and are found around 20°N close to the continental margin (*Brandt et al.* [2015]).

Oxygen concentrations in the ocean are governed by a balance of oxygen-consumption by biogeochemical processes, and oxygen supply through ventilation at the atmosphere/ocean interface and both biogeochemical and physical processes (e.g. *Wyrtki* [1962]). As such, oxygen as a tracer is not conserved and undergoes multiple changes along its path originating from their subduction region. Biogeochemical processes are not subject of this work and will therefore not be discussed in detail here. Physical processes include, but are not limited to, the lateral advection of oxygen-rich waters in ocean currents, e.g. in zonal

current bands advecting higher-oxygen waters from the western boundary (*Brandt et al.* [2010]), and the vertical advection through diapycnal mixing (*Banyte et al.* [2012]; *Fischer et al.* [2013]) or upwelling of deeper, oxygen-richer waters (e.g. *Brandt et al.* [2015]). The shallow naOMZ generally shows higher oxygen concentrations than the deep oxygen minimum (*Brandt et al.* [2015]), although very low concentrations are observed periodically. Due to its vicinity to the highly productive upwelling region off Mauritania (e.g. *Brandt et al.* [2015]), the main cause for the existence of the shallow oxygen minimum is considered to be oxygen consumption through remineralization related to enhanced primary productivity in the surface layers and shallow mixed-layers (*Karstensen et al.* [2008]).

The Mauritanian upwelling region (MUR) is part of the Canary upwelling system that extends from 10°N to 43°N (e.g. *Mittelstaedt* [1991]). It is one of the four major eastern boundary coastal upwelling systems in the world oceans, together with the Peru (e.g. *Brink et al.* [1983]) and California (e.g. *Marchesiello et al.* [2003]) upwelling systems in the tropical South and North Pacific as well as the Benguela upwelling system in the tropical South Atlantic. The seasonality of coastal upwelling in the MUR has previously been described in detail by e.g. *Mittelstaedt* [1983], *Van Camp et al.* [1991] and *Lathuilière et al.* [2008]. Between 12°N and 20°N the seasonal migration of the intertropical convergence zone (ITCZ) drives pronounced seasonality of upwelling-favorable alongshore winds resulting in the main upwelling season lasting from December to April (*Mittelstaedt* [1983, 1991]; *Barton et al.* [1998]; *Brandt et al.* [2015]). During that time the MUR exhibits high productvity in surface layers due to the supply of cold, nutrient-rich waters to the shelf region. Upwelled waters in the MUR are mostly comprised of water masses with South Atlantic origin (e.g. *Mittelstaedt* [1983, 1991]; *Peña-Izquierdo et al.* [2015]).

The three main water masses encountered in the MUR and over the depth ranges of the shallow and deep oxygen minimum zones, which are therefore the main focus of this study, are the tropical surface water (TSW), the North and South Atlantic central waters (NACW,SACW) and the Antarctic intermediate water (AAIW). Waters with potential densities $\sigma_\Theta \leq 25.8 kgm^{-3}$ (e.g. *Stramma et al.* [2008a]) belong to the TSW water mass. This water mass is usually rich in oxygen (e.g. *Karstensen et al.* [2008]), due to its direct contact with the atmosphere. Below the TSW, a strong oxycline separates the TSW from the central waters.

The NACW and SACW have potential densities between $\sigma_\Theta = 25.8 kgm^{-3}$ and $\sigma_\Theta = 27.1 kgm^{-3}$ (e.g. *Stramma et al.* [2005, 2016]). The upper density bound is set by the wintertime surface density distribution in the winddriven, subtropical gyres (*Luyten et al.* [1983]; *Karstensen et al.* [2008]), where they are formed by subduction through Ekman

convergence and associated Ekman pumping. Only waters subducted in winter or spring have densities and vertical Ekman velocities high enough to leave the mixed-layer and be permanently subducted into the thermocline. They are further characterised by a near-linear potential temperature and salinity relationship. The NACW is relatively warm and saline, while the SACW is colder and fresher. The two water masses differ in their biogeochemical properties as well. NACW shows higher oxygen concentrations, since it is more recently ventilated compared to the SACW (e.g. *Peña-Izquierdo et al.* [2012]) and the SACW is generally higher in nutrients, such as nitrate (*Schafstall* [2010]). In the ETNA the NACW and the SACW are separated by the Cape Verde frontal zone (CVFZ) (e.g. *Tomczak* [1981]; *Zenk et al.* [1991]), located at around 20°N at the West African coast, oriented southwestwards down to about 16°N just north of the Cape Verde Islands and coinciding with the NEC transporting NACW southwestward (*Brandt et al.* [2015]). Since the two central water masses occupy the same density stratum, exchange through filaments, eddies and other meso- and submesoscale features across the front is common (*Tomczak* [1981]; *Stramma et al.* [2005]; *Pastor et al.* [2012]; *Schütte et al.* [2016]). The central water masses can be further divided into a lower central water (lCW) and upper central water (uCW) (e.g. *Elmoussaoui et al.* [2005]; *Peña-Izquierdo et al.* [2012]; *Fischer et al.* [2013]; *Peña-Izquierdo et al.* [2015]). The change from uCW to lCW generally coincides with a salinity minimum and a temperature inversion in the region. The isopycnal surface commonly defined to separate the two is $\sigma_\Theta = 26.8 kgm^{-3}$ (e.g. *Rhein et al.* [2005]; *Kirchner et al.* [2009]). South of 15°N, SACW is found to dominate the uCW layer (*Rhein et al.* [2005]; *Kirchner et al.* [2009]), while a mixture of NACW and SACW can be found in the uCW in the entire region (e.g. *Voituriez and Chuchla* [1978]; *Peña-Izquierdo et al.* [2012, 2015]). On its way north from its subduction region in the subtropical gyre of the South Atlantic, the SACW is taking a path via the North Brazil Current, the North Equatorial Undercurrent and eventually the Poleward Undercurrent (*Glessmer et al.* [2009]; *Schütte et al.* [2016]).

Below the central water masses, occupying the density stratum between $\sigma_0 = 27.1 kgm^{-3}$ and $\sigma_1 = 32.15 kgm^{-3}$ (*Stramma et al.* [2008a]), lies the AAIW. In the tropical Atlantic ocean it is characterized by a minimum in salinity between 600 to 900m depth (*Stramma et al.* [2005]) that can be traced to latitudes up to 24°N (*Reid* [1994]). Created in the subpolar latitudes around Antarctica, the AAIW spreads into all ocean basins (*Reid* [1994]). *Pastor et al.* [2012] showed that AAIW dominates the intermediate water layer close to the continental slope off Northwest Africa and forms a nutrient maximum at depth.

The MUR is a region of high mesoscale activity and variability (*Karstensen et al.* [2015])

with cyclonic and anticyclonic eddies frequently generated at the eastern boundary (*Schütte et al.* [2016]) dominating the velocity field. The mean horizontal circulation and hence the ventilation of the shadow zone/OMZ in the MUR occurs mainly through the surface Mauritania Current (MC) and the Poleward Undercurrent (PUC) below. Additionally, weak zonal current bands further act to ventilate the OMZ in the central water and AAIW layers (*Stramma et al.* [2005, 2008a]; *Brandt et al.* [2010]).

The general charateristics of the PUC were previously described by e.g. *Mittelstaedt* [1983], *Barton* [1989] and *Peña-Izquierdo et al.* [2012] through hydrographic and current measurements. The PUC is generally considered to originate from the Gulf of Guinea region flowing at speeds between 5-20cms^{-1} (*Mittelstaedt* [1983]), fed by the North Equatorial Countercurrent (NECC) and its northern branch, the northern NECC (nNECC) as well as the North Equatorial Undercurrent (NEUC) (*Stramma et al.* [2008a]). With a width of 30-60km it flows poleward attached to the continental slope at depths between 50-300m, periodically extending to depths as deep as 1000m (*Mittelstaedt* [1983]; *Barton* [1989]; *Peña-Izquierdo et al.* [2012]). The dominant forcing mechanism for the PUC is northward Sverdrup transport induced by positive wind stress curl (*Mittelstaedt* [1983]), comparable to other major eastern boundary current systems such as the California Current System (*McCreary Jr. et al.* [1987]; *Marchesiello et al.* [2003]; *Capet et al.* [2004]) or the Peruvian Upwelling Region (*Albert et al.* [2010]; *Echevin et al.* [2011]; *Chaigneau et al.* [2013]). A major influence of coastal Kelvin waves on the near-coastal circulation like in the Benguela Upwelling Region (*Fennel* [1999]) or the Peruvian Upwelling Region (*Brink et al.* [1983]; *Echevin et al.* [2014]) could so far not be shown (*Polo et al.* [2008]). The seasonality in PUC intensity as well as its presence should therefore be directly related to the local wind stress curl off the coast. Once reaching the latitudes of the subtropical gyre circulation, the PUC reportedly deepens and continues flowing northward underneath the CC (*Mittelstaedt* [1983]).

The surface MC, often described as indistinguishable from, or rather the surface manifestation of, the PUC (*Mittelstaedt* [1983]; *Peña-Izquierdo et al.* [2012]), shows seasonality due to prevailing southward winds during the uwelling season and the seasonality of the intensity of the northern equatorial current bands related to the meridional migration of the ITCZ. Two possible explanations for the origin of this countercurrent include the meridional pressure gradient developing due to the migration of the CC away from the northwest African coast the zonal equatorial current bands impinging on the eastern boundary in the south, as well as excess rainfall and river discharge in that region (*Mittelstaedt* [1976, 1983]; *McCreary Jr. et al.* [1987]). During the summer and autumn months, when trade winds are weaker and the NECC is at its strongest, the MC report-

edly reaches latitudes of up to 20°N (*Mittelstaedt* [1991]). However, during the upwelling season, the MC only reaches latitudes of about 14°N. The surface MC can be seen as an extension of the nNECC as it impinges onto the west African coast at around 10°N. Both the MC and the PUC transport relatively low-salinity and nutrient-rich, warm and with respect to the OMZ waters oxygen-rich, central waters of south Atlantic origin into the OMZ (e.g *Voituriez and Chuchla* [1978]; *Stramma et al.* [2008a]; *Peña-Izquierdo et al.* [2012]; *Brandt et al.* [2015]) and should therefore play an important role in the ventilation through lateral advection. In fact, it is this cross-equatorial exchange of water masses that *Karstensen et al.* [2008] see as the main reason for the prevention of suboxic conditions in the naOMZ. The seasonality in both the the MC and the PUC must be reflected in the hydrography and water mass characteristics in the MUR as well as play a not negligible role in the oxygen supply in the central water stratum over the continental slope and shelf in the study area.

Mittelstaedt [1983] proposed the existence of an anticyclonic gyre-like circulation cell caused mainly by variations in wind forcing. He described the MC being the northward branch and extensions of the CC supplying the recirculation pathway away from the coastal region. Modelling studies seem to be able to reproduce the feature and regional low oxygen concentrations point towards such a circulation cell (*Stramma et al.* [2008a]; *Brandt et al.* [2015]; *Stramma et al.* [2016]). The resulting tracks of three drifters deployed near Cape Blanc at 100m water depth were described to support this circulation pattern by *Peña-Izquierdo et al.* [2012]. The recirculation should therefore be a seasonal circulation feature in the region. *Peña-Izquierdo et al.* [2015] used ECCO2 model simulations as well as observational hydrographic data to study water mass pathways into the naOMZ. They observed a cyclonic circulation cell in the upper central water layer and further proposed the existence of an anticyclonic circulation cell in the lower central water layer, based also in part on observations of water mass properties described in *Peña-Izquierdo et al.* [2012]. *Peña-Izquierdo et al.* [2012] studied the near-coastal circulation over the continental slope and shelf between the Canary and Cape Verde Islands in the upper 600m of the water column using hydrographic, oxygen and velocity data from one research cruise conducted in November 2008. Their observations agreed well with current conditions previously described by *Mittelstaedt* [1976], concluding that currents observed during their cruise represented typical late summer and autumn conditions.

The main objective of this present study is to describe to seasonality of the boundary circulation, associated water mass changes in the MUR and its connection to seasonal variations of cyclonic wind stress curl along the coast. Further, the role of these seasonally renewed water masses in the ventilation of the OMZ in the shadow zone of the

ETNA is investigated. For the first time an extensive observational data set combining acoustic current measurements as well as hydrographic and oxygen data covering several months and seasons is available to describe the seasonality of the subsurface poleward undercurrent, water masses and oxygen content in this socio-economically and ecologically important part of the ETNA. An understanding of the seasonality of the aforementioned parameters is crucial for understanding how it may behave under a changing climate scenario.

This work is organised as follows. First, the data and methods employed for analysis in this study are described in section 2. Following is a general description of the seasonal atmospheric forcing and the oceanic response in the MUR. Results from the described analysis are presented in section 4, followed by a description of the larger-scale seasonal circulation in the tropical gyre on the basis of Sverdrup dynamics in section 5. A general discussion of the presented results in the context of other publications as well as a conclusion and outlook conclude the study in sections 6 and 7.

2 Data and Methods

Data sets from various in-situ and remote platforms were used for analysis in this work and will be described in this section.
Among them, a unique dataset of shipboard hydrographic, oxygen and acoustic current measurements in the water column from nine research cruises is the main basis for analysis. Further, climatological hydrographic and oxygen data as well as various satellite products are used. The methods used to analyse the data sets are briefly described.

2.1 Shipboard Measurements

Hydrographic, oxygen and acoustic current measurements are available from nine research cruises in the eastern tropical North Atlantic undertaken within the framework of various projects between 2005-2016 to study the hydrography and the circulation in the Mauritanian upwelling region. Table 1 summarises the cruises, their duration, sections used to obtain mean sections of velocities and hydrography, and the total number of CTD-O_2 profiles taken during each cruise. CTD-O_2 profiles include measurements of temperature, salinity, pressure and oxygen concentration. Five cruises (P320, P347, P348, ATA3, MSM17/4) were carried out during winter and early spring, during which coastal upwelling was present in the study area. The remaining four cruises (M68/3, P399, M107, M129) were carried out after the upwelling season during the summer months.

Upper ocean current velocities in the water column were recorded using the vessel-mounted acoustic Doppler current profiler (vmADCP) on the respective research vessel. Vertical range and resolution vary, but in general good quality velocity data is available

Cruise short	Ship	Period	Sections [°N]	no. of CTD/O_2 profiles
P320	*RV Poseidon*	Mar - Apr 2005	17 - 19	43
M68/3	*RV Meteor*	Jul - Aug 2006	17.5 - 19	95
P347	*RV Poseidon*	Jan - Feb 2007	17.5 - 18.5	126
P348	*RV Poseidon*	Feb 2007	18 - 19	33
ATA3	*RV L'Atalante*	Feb 2008	17 - 19	61
P399	*RV Poseidon*	Jun 2009	18	25
MSM17/4	*RV Maria S. Merian*	Mar - Apr 2011	18	69
M107	*RV Meteor*	Jun 2014	18	73
M129	*RV Meteor*	Aug 2016	17.6 - 18.6	68
				Σ 593

Table 1: *Data from these research cruises is used for analysis throughout this work.*

from the 75kHZ unit for depths between 25-750m with a vertical resolution of 8m as 1-minute averages. The vmADCP produces estimates of meridional (v) and zonal (u) velocities as well as backscatter amplitudes. Because of the varying vertical resolution, data from the different cruises is interpolated onto a uniform grid with a 10m vertical and 1/100° horizontal resolution. For the specific instruments used during the individual cruises, accuracies of the measurements after calibration and other detailed descriptions the reader is referred to the individual cruise reports.

Since not all cruises cover the same zonal sections and CTD-O_2 station density and in order to obtain comparable sections of current velocities and hydrography between 17°N and 19°N, velocities and CTD-O_2 measurements are interpolated onto a reference grid representing the topography at 18°N. This latitude was chosen, because it coincides with the highest density of measurements from all cruises (see Figure 1) and borders on the climatologically lowest oxygen concentrations found in the shallow OMZ. Velocities are rotated into their respective cross- and alongshore velocity components. Angles are extracted from ETOPO data in 1-minute horizontal resolution (source: *https://www.ngdc.noaa.gov/mgg/global/global.html*) and range from 20°T at 17°N to -40°T at 19°N. The topography along the sections was obtained by identifying the bottom signal in backscatter amplitude from vmADCP measurements. Depending on the range of the instrument and quality of the data the bottom signal was identifyable to a depth of around 600 to 700m. For deeper and shallower depths than the range of the vmADCP the continental slope and shelf were extrapolated. A comparison with the ETOPO-18°N section validates this method. Using these topographies, velocities at different latitudes are projected onto the topography at 18°N to account for meridional changes of the shelf break and shelf width. This is done since the eastern boundary currents follow f/H contours due to potential vorticity constraints (e.g. *Chaigneau et al.* [2013]). Since the main objective of these analyses is to accurately represent the hydrographic properties carried alongshore in these currents, profiles of temperature, salinity and oxygen are handled in the same manner. This yields estimates of the circulation and hydrographic conditions during the individual cruises, which are then averaged into a winter (five cruises) and a summer (four cruises) seasonal mean section. The method employed to define the seasonal means will be described in section 4.

Volume transport within the boundary currents is calculated by integrating alongshore (positive northward) velocities in a box from the coast to a distance 60km (17°W at 18°N) from the 100m-isobath (the depth of the shelf break). Vertically, transports are calculated for uCW and SW (down to about 250m water depth), and lCW (between 250m and 450m) layers separately. Positive/negative alongshore velocities are integrated

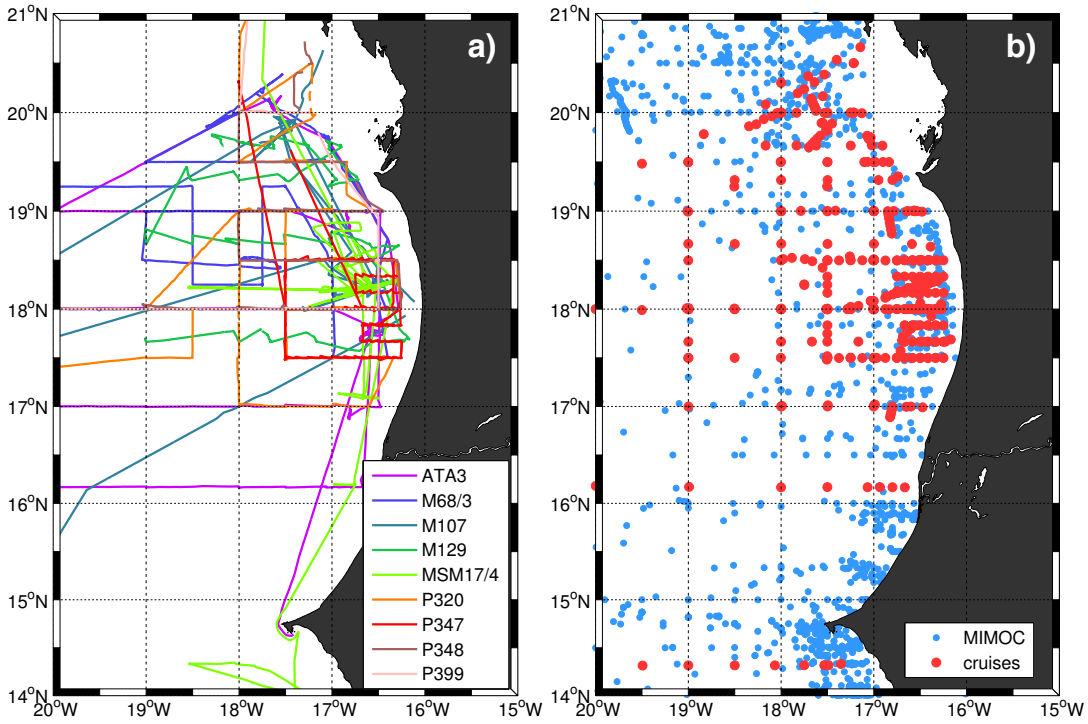

Figure 1: *(a) Cruise tracks of the individual research cruises and (b) available hydrographic stations from nine cruises (red dots) and MIMOC (blue dots) (Schmidtko et al. [2013]) used for analysis in this study.*

for the upper/lower layers. Transports are calculated in *Sverdrup* ($[Sv] = 10^6 m^3 s^{-1}$).

2.2 Climatological Hydrographic Data

Cimatological hydrographic and oxygen data is available in gridded form from the monthly isopycnal/mixed-layer ocean climatology (MIMOC). For a full description of the methods and data quality checks the reader is referred to *Schmidtko et al.* [2013]. A total of 2006/1458 CTD profiles without/with oxygen measurements is available between 14°N - 21°N and 20°W - 15°W down to a depth of 2000m and is used for analysis to supplement the cruise data (Fig. 1b).

2.3 Oxygen Units

Values of oxygen concentration in this study are given in $[\mu molkg^{-1}]$. For cruise M68/3 oxygen concentrations are given in mll^{-1} and a conversion of the two units is done following e.g. *Karstensen et al.* [2008] and *Ekau et al.* [2010]:

$$O_2(\mu molkg^{-1}) = 44.66(\mu molml^{-1}) \times O_2(mll^{-1})/\sigma(kgm^{-3}).$$

Here, σ is the potential density of the water sample calculated from CTD data at which the oxygen sample was taken.

2.4 Water Mass Analysis

The aforementioned linear potential temperature (Θ)-S relationship of the South and North Atlantic central water wasses allows for a composition analysis of individual water parcels throughout the respective potential density range (e.g. *Johns et al.* [2003]; *Peña-Izquierdo et al.* [2012, 2015]). Water mass analysis is performed within the central water stratum to analyse the relative contributions of SACW and NACW to a given water sample measured with the CTD. The method to obtain typical salinity properties on isopycnal surfaces, from which the relative contributions of the South and North Atlantic central water masses can be estimated, described by *Johns et al.* [2003] is not applicable in the MUR. The previously mentioned water mass change at the boundary between the uCW and lCW (Fig.2) would lead to an overestimation of SACW contribution in that layer. Hence a linear Θ-S relationship that best fits the observed data is assumed based on the description in *Schafstall* [2010] (see Tab.2).

Available salinity data from CTD measurements within the central water stratum in the study area is analysed for relative contributions of central waters of South and North Atlantic origin on its respective isopycnal surface. This analysis aids in analysing the water mass distribution in the PUC and shelf region during the individual cruises and its seasonal variability.

	SACW	**NACW**
lower/upper **S**	35.1/35.65	35.37/37
lower/upper $\Theta\,[^\circ C]$	9.6/17.9	10.8/21.8

Table 2: *Lower and upper limits of salinity (S) and potential temperature (Θ) defining the linear relationship in the central water stratum used for water mass analysis.*

The relative contribution of SACW to a given water parcel is given by

$$SACW[\%] = \frac{S_{NACW} - S_{CTD}}{S_{NACW} - S_{SACW}} \times 100,$$

where subscript indices *NACW/SACW* indicate characteristic North/South Atlantic central water salinities on a given isopycnal and *CTD* is the measured water sample at that isopycnal, following the method described in *Johns et al.* [2003].

Since both the NACW and the SACW occupy the same density stratum, intrusions of water parcels of either hemispheric origin can be found in CTD sections along the continental margin.

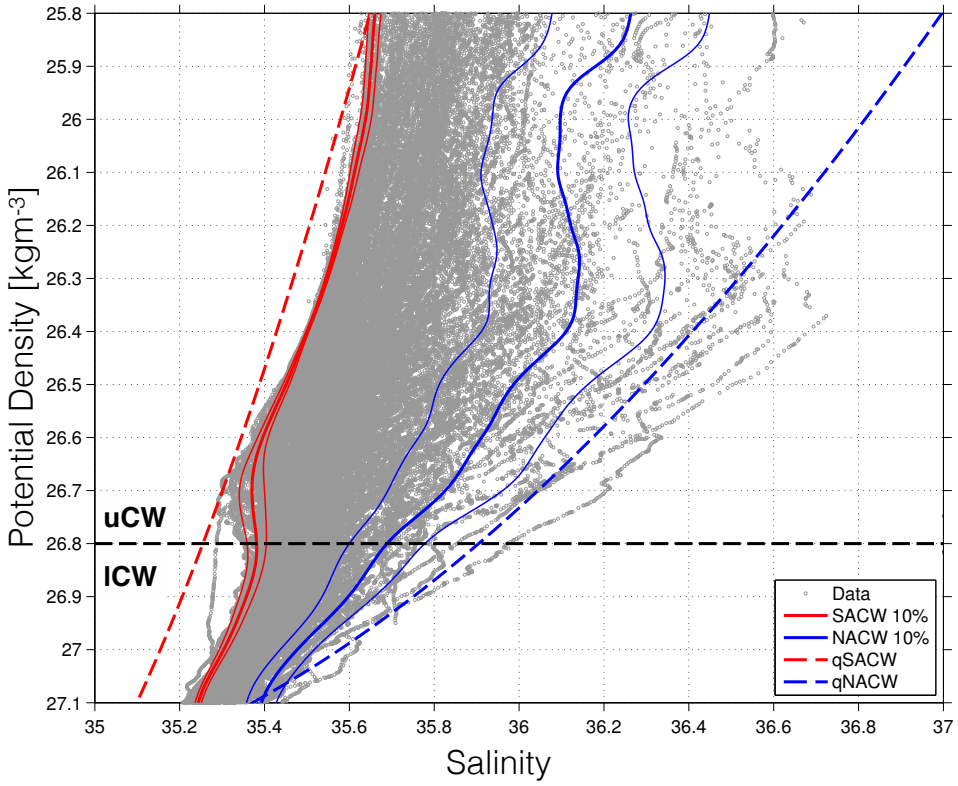

Figure 2: *Potential density (σ_Θ)-Salinity diagram. Data points include all available hydrographic measurements in the Central Water stratum from nine cruises. Thick blue/red lines define typical NACW/SACW characteristics calculated using the method described in Johns et al. [2003]). Thin colored lines define ±1 standard deviation. Blue/red dotted lines define typical NACW/SACW characteristics assuming a simple linear relationship in Θ-S space used for water mass analysis in this study. The 26.8kgm^{-3}-isopycnal separates the upper and lower central water layers.*

2.5 Satellite Products

Various satellite products are used in the following sections to describe the oceanic response to the seasonal atmospheric forcing in the study area and to establish a connection to the observed hydrographic and current conditions later on. Satellite products include sea surface temperatures, surface cholorophyll concentrations as well as wind velocities from which wind stress and wind stress curl are calculated.

2.5.1 Wind Products

The Scatterometer Climatology of Ocean Winds (SCOW) is used in the following section for a general description of the seasonal wind forcing in the region. SCOW is based on 122 months of QuickSCAT data from September 1999 through October 2009. Due to the rather short available time series, SCOW uses harmonic analysis instead of regular arithmetic averaging to obtain monthly averages. For a detailed description of the methodology to obtain this monthly climatology the reader is referred to *Risien and Chelton* [2008]. QuickSCAT surface winds are downloaded from *ftp://ftp.ssmi.com/qscat/bmaps_v04/* as weekly averages from January 2005, to coincide with the observation period within our cruise data, until November 2009, when the product expired. ASCAT surface winds are available from 2007 until present and were downloaded as weekly averages from *ftp://ftp.ssmi.com/ascat/metopa/bmaps_v02.1/* (most recent data downloaded on September 4^{th} 2016; unregistered data access has been disabled as of December 12^{th} 2016). Wind stress is calculated from 10m ASCAT/QuickSCAT winds at a 1/4° horizontal resolution following *Large and Pond* [1981].

Meridional Sverdrup transport is calculated from the wind stress curl following *Sverdrup* [1947] by integrating

$$M_y = \frac{1}{\beta\rho_0}\hat{k}\cdot(\nabla\times\tau)\,,$$

from the coast to 17°W. For the sake of better comparability, this boundary coincides with the integration boundary of the ship transports. $\beta = 2.3\times10^{-11}s^{-1}m^{-1}$ is the change of the coriolis parameter f with latitude, $\rho_0 = 1025kgm^{-3}$ is a reference density and $\hat{k}\cdot(\nabla\times\tau)$ is the z-component of the wind stress curl vector.

A Sverdrup transport streamfunction ψ is defined by

$$\beta\frac{\partial\Psi}{\partial x} = \frac{1}{\rho_0}\hat{k}\cdot(\nabla\times\tau)\,.$$

Integrating this relation from the eastern boundary x_0 to a point x yields the desired streamfunction at point x:

$$\Psi(x) = \frac{1}{\beta\rho_0} \int_{x_0}^{x} \hat{k} \cdot (\nabla \times \tau)\, dx$$

Here it is assumed that at the eastern boundary $\psi(x_0) = 0$. The streamfunction is given in units of $[Sv]$.

A problem with these data sets is the poor near-coastal coverage. In general around one to two grid points are missing towards the coast, leading to an underestimation of the wind stress curl in these dynamically important regions. Estimates of northward Sverdrup transport calculated from wind stress curl should be seen as an estimate of order of magnitude, rather than precise calculations or values. The poor data quality and coverage is a problem because of near-shore equatorward currents driven by along-shore wind stress and poleward currents driven by positive wind stress curl (e.g. *Marchesiello et al.* [2003]; *Capet et al.* [2004]).

2.5.2 Sea Surface Temperature

Sea surface temperature (SST) is a good indicator of coastal upwelling. In this study microwave radiometer data available from Remote Sensing Systems (*www.remss.com*) is used. The product, called Microwave Optimally interpolated Sea Surface Temperature, combines all available radiometer measurements in a given day and is available in a gridded 9km horizontal, daily resolution. Measuring in the microwave spectrum, clouds do not affect the data quality and good data is available from 2005 to 2015. SST is used to compute an uwelling index (UI) as a proxy for upwelling intensity close to the coast. The UI is defined as the differences in SST between the coast and a point 500km offshore (*Nykjaer and Van Camp* [1994]).

2.5.3 Chlorophyll-A Concentrations

Chlorophyll is used as a metric to estimate primary productivity in the surface layer during upwellling season and the remainder of the year. High resolution satellite data from MODIS-Terra is available from *www.oceandata.sci.gsfc.nasa.gov*, downloaded as monthly climatological data gridded in a 9km horizontal resolution. The climatological data set is based on measurements from 2000 to present (most recent data downloaded on November 28^{th} 2016). A chlorophyll extension index (CEI) is defined as the distance from the

coast, where surface chlorophyll concentrations exceed six times the average concentrations found between 1200km-1500km offshore (based in part on the method described by *Lathuilière et al.* [2008]).

2.5.4 Geostrophic Surface Velocities

Absolute geostrophic velocities at the sea surface are derived from absolute dynamic topography measurements. The delayed-time data set is produced by Ssalto/Duacs and includes merged data from all available satellite measurements between 1993 and early 2016. The gridded product is available from AVISO (*www.aviso.altimetry.fr/duac/*) in a 1/4° horizontal, daily resolution. Data is downloaded for 2005-2015 and averaged monthly.

2.6 Seasonal Cycle

In order to investigate the seasonal as well as spatial variability in the SST UI, surface chlorophyll concentrations and the CEI, Hovmöller diagrams for a climatological year between 14°N - 22°N are plotted. The daily SST UI data set is smoothed over 10 days and $30km$ to exclude high frequency signals following *Lathuilière et al.* [2008]. Since the chlorophyll data set already contains climatological values, no further smoothing in the time domain is performed. In the meridional direction, the same smoothing scale as for the SST UI is chosen. Chlorophyll concentrations are averaged in a band of 200km width along the coast.

3 Oceanic Response to Seasonal Atmospheric Forcing

In this section the atmospheric forcing, namely meridional wind stress and wind stress curl, and its effect on oceanic parameters such as SST and surface chlorophyll concentrations through near-coastal winddriven upwelling are briefly discussed. The objective hereby is not to focus on individual years, but to give a general overview on the seasonality and a brief discussion on the connection of the atmospheric forcing and the observed oceanic reasponse on a seasonal timescale.

The main driver of winddriven coastal upwelling of nutrient-rich waters and hence primary productivity in the surface layer in any eastern boundary costal upwelling region is the wind stress. More precisely, the along-shore wind stress component induces offshore Ekman transport and a successive supply of colder, nutrient-rich waters to the surface

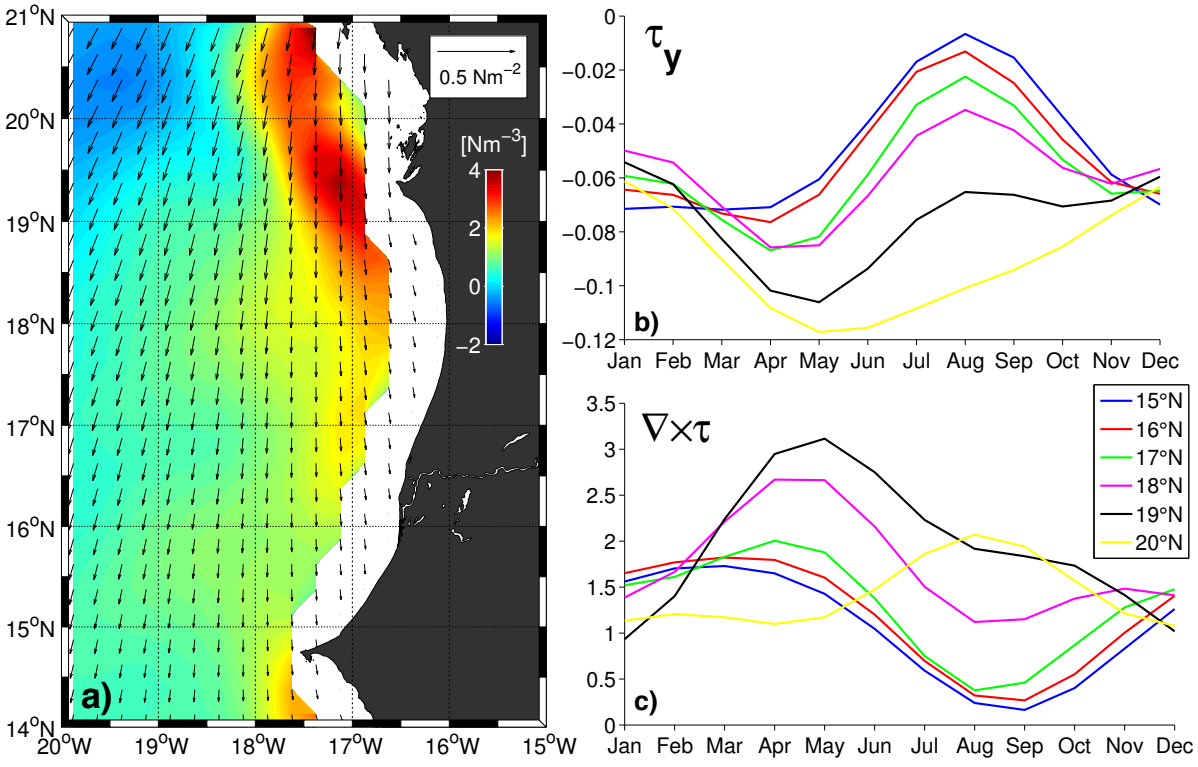

Figure 3: *Climatological wind data from SCOW based on satellite data between 1999-2009: (a) Annual mean wind stress τ (arrows) and wind stress curl $\nabla \times \tau$ (colors, in $10^{-7} Nm^{-3}$), (b) seasonal meridional wind stress along different latitudes in a band 200km offshore and (c) seasonal wind stress curl (in $10^{-7} Nm^{-3}$) in the same band. Colored lines in (b,c) indicate different latitudes according to the legend in (c). Note that wind stress in (b) is negative, i.e. the y-axis compared to (c) is flipped.*

(*Brink* [1983]). The near-shore region of the MUR is characterised by positive (cyclonic) wind stress curl year-round, with maximum curl north of 19°N (Fig.3a). Meridional wind-stress in the MUR shows a seasonal cycle due to the seasonal migration of the ITCZ. This seasonality is most pronounced between 15°N - 18°N, with maximum southward wind-stress occurring until late spring in April-May, followed by a sharp decrease to minimum values in August (Fig.3b). Meridional wind stress at 19°N shows a less pronounced seasonality with generally higher values throughout the year, while at 20°N, maximum wind stress in May is followed by a period of slowly decreasing values for the rest of the year. Wind stress curl also shows a seasonal cycle, in phase with the meridional wind stress for latitudes below 19°N. Wind stress curl shows highest values at 18°N - 19°N, reaching its maximum in May, while at 20°N the maximum is reached in August-September (Fig.3c). Between 17°and 18°-19°N there is an increase in wind stress curl magnitude, that seems to be a consistent feature around the headlands of Cape Blanc and off the Banc d'Arguin throughout the year (Fig.3a). This increase in wind stress curl would lead to a divergence in Sverdrup transport south of 18°N and a convergence north of 19°N. Additionally, a

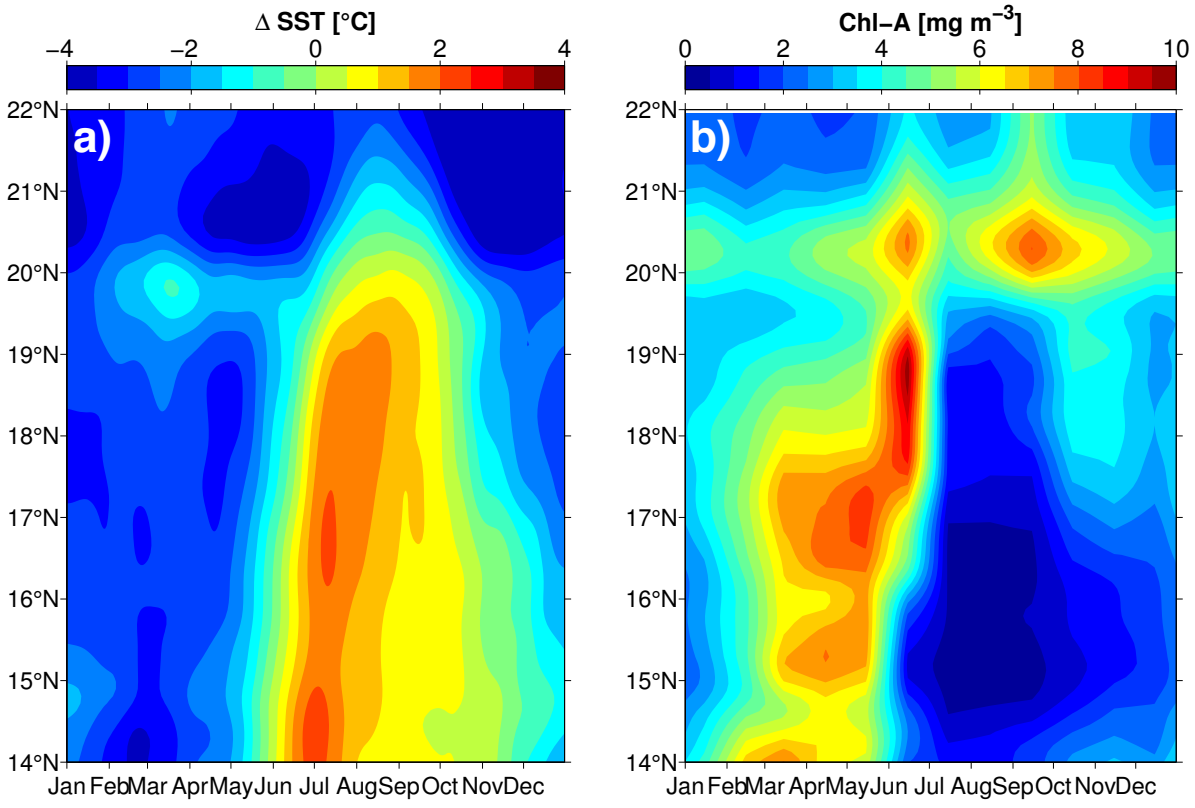

Figure 4: *(a) SST upwelling index defined as the difference in SST between the coast and 500km offshore. Upwelling index is calculated for the period between 2005-2016. (b) Climatological chlorophyll-A concentrations* $[mgm^{-3}]$ *in a band 200km from the coast from MODIS with a 9km resolution.*

secondary, albeit smaller, maximum at 18°N and 19°N can be seen in the climatological data. The fact that this maximum is less pronounced than the late spring maximum could point to interannual variability in wind stress curl intensity during the beginning of the upwelling season in late autumn. The period from April/May to August/September associated with an abrupt decrease in meridional wind stress, thus ending the upwelling season, as well as wind stress curl has been termed the *relaxation season* by *Lathuilière et al.* [2008], which will be referred to by the same term and will receive special focus during the remainder of this study as well.

The SST UI for the MUR shows a very clear upwelling signal, with negative UI values, i.e. colder SSTs close to the coast compared to off shore, prevailing until May-June south of 20°N (Fig.4a). Minimum UIs are found between 17°N - 19°N towards the end of the upwelling season in April/May, coinciding with maximum meridional wind stress at these latitudes. An abrupt warming of near-coastal SSTs is observed in May-June, coinciding with the sudden decrease in meridional wind stress at these latitudes (cf. Fig.3b). Due to

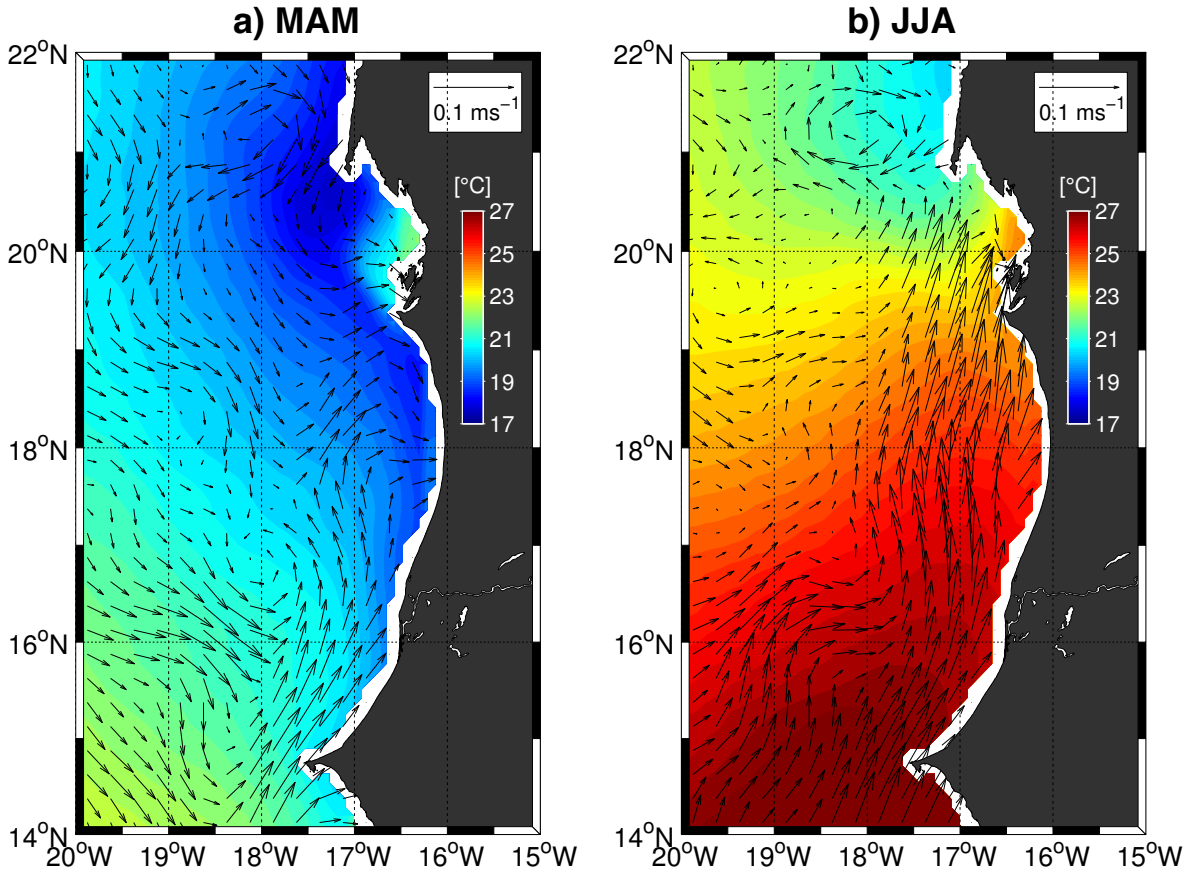

Figure 5: *Climatological SSTs (colors) and geostrophic velocities (arrows) from satellite data for months (a) March, April, May and (b) June, July, August. Arrow in top right corner of both panels depicts reference length for 0.1ms^{-1}.*

its intensity and rapid warming occurring over the course of just a few weeks, it must at least in part be forced dynamically through advection of warmer surface waters from the south in the surface currents. This is further apparent in this warming signal seemingly propagating northward, with strong warming in the south occurring almost a month prior to the north. Geostrophic surface velocities show northward velocities reaching as far as 16°N towards the end of the upwelling season (MAM, Fig.5a), when cold SSTs prevail along the coast, while during the relaxation season, rapid warming occurs and strong northward velocities reach 20°N. These strong surface currents, associated with a weakening of southward wind stress and seasonal strengthening of the nNECC in the south, advect warm waters northward and are likely connected to the surface MC. North of 20°N, upwelling signals can be seen throughout the year with strongly negative SST UIs. Slightly warmer UIs between July-September are probably related to the surface MC reaching further north during the period of minimal meridional wind stress. The blob of higher SST UI just south of 20°N between March-April is likely a signature of the warm Banc d'Arguin water (e.g. *Tomczak* [1981]; *Van Camp et al.* [1991]) intruding into the off-shore region.

The seasonality of surface chlorophyll concentrations generally shows the same patterns. South of 20°N surface chlorophyll increases from 0-2mgm^{-3} in August/September to 10mgm^{-3} in June. Minimum SST UIs lead maximum chlorophyll concentrations in the surface layer, when strongest upwelling occurs (Fig4b), and chlorophyll remains high until approximately June, lagging the observed decrease in SST UI by about a month. This suggests that in the absence of strong northward surface currents, chlorophyll concentrations are able to remain high even after upwelling-favorable winds have seized. However, following the rapid warming observed close to the coast, surface chlorophyll decreases drastically over the course of a few weeks as well, further pointing to the advection of warm, chlorophyll-poor waters from the south. Between 20°- 21°N, enhanced chlorophyll concentrations between 4-

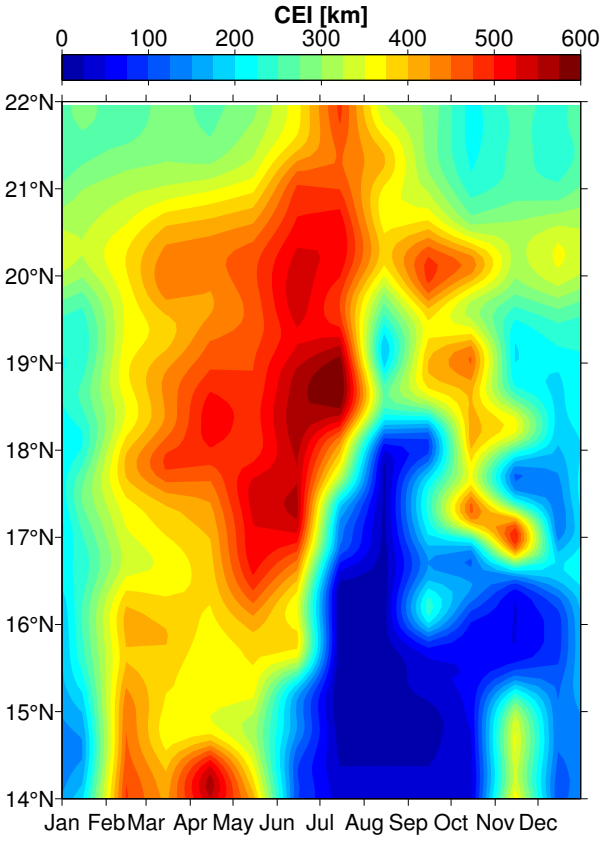

Figure 6: *Chlorophyll extension index (CEI) from climatological surface chlorophyll concentrations.*

$8mgm^{-3}$ are observed throughout the year and are likely associated with the *giant filament* (e.g. *Van Camp et al.* [1991]).

The offshore extension of waters with high surface chlorophyll concentrations (Fig.6) shows the same seasonal patterns as the SST UI or the surface chlorophyll. The CEI also reflects the advection of upwelled waters high in chlorophyll and nutrients offshore through Ekman dynamics. South of 19°N the CEI ranges from 10km during the relaxation season to almost 600km towards the end of the upwelling season. Between 18°- 19°N enhanced chlorophyll concentrations farthest offshore in June coincide with highest chlorophyll concentrations found close to shore during that time, remaining high well into July. This expansive and extended offshore extension well into the relaxation season must affect the remineralisation of oxygen in the subsurface layers as well.

The good seasonal agreement between the SST UI and surface chlorophyll concentrations in the near-shore region highlights its connection to the wind forcing, while the sudden warming and decrease in chlorophyll points to a dynamically driven process, such as advection of waters from the south. It further suggests the absence of a strong impact on near-shore surface productivity of coastally trapped waves in the region (*Lathuilière et al.* [2008]) as was shown by e.g. *Echevin et al.* [2014] for the Humboldt Current System off Peru. Further offshore, the advection of nutrient-rich upwelled waters extends surface productivity well inot the relaxation season.

4 Results

In this section the main findings of this study will be presented. The presentation will be consecutive, starting with the boundary circulation, the water masses that are carried by it and the effect on the oxygen concentration, followed by a closer look at the meridional penetration of water mass characteristics and oxygen concentrations in the boundary currents.

4.1 Boundary Circulation

The boundary circulation is analysed using the nine ship sections of meridional velocities interpolated onto the topography at 18°N. The currents close to the shelf break are analysed and their seasonal variability described. Additionally, the seasonality of isopycnal surfaces, calculated from available CTD measurements along the sections, is discussed in the context of the observed circulation over the slope and shelf. Further, periods for the calculation of seasonal mean sections are defined and the circulation during two distinct regimes presented.

Enhanced northward velocities were observed during summer cruises, with most intense current velocities in excess of 40-50cms^{-1} (M68/3, P399) confined to the SW and upper uCW layers above 100-150m water depth (Fig.7). The lower part of the northward flow along the boundary, likely associated with the PUC beneath the surface layer, stays attached to the slope right around the 100m isobath, while the upper part seems to meander zonally across several tens of kilometers. During P399 the strongest velocities were confined to a very distinct core above 100m water depth, detached from the slope. This detachment is likely due to instability of the boundary current. During M68/3 the flow is attached to the slope and spreads across the shelf region, with strongest velocities right around the 50m isobath. The strong surface-intensified northward currents extending over the shelf are connected to an eddy forming at 18°N. However, the section at 19°N (not shown), which is included in this mean section, shows even stronger flow and no sign of eddy activity, therefore pointing to the presence of an intensified northward current. During M107 northward velocities extended over the entire shelf and most of the uCW as well as parts of the lCW layer far offshore. M129 exhibits only a small northward velocity component confined mostly to the surface layer detached from the slope and shelf. Over the shelf we find strong southward velocities. However, the shape of this small velocity core resembles the general tilted shape of the northward flow during the summer cruises and might be a remnant of a stronger flow prior to the period of

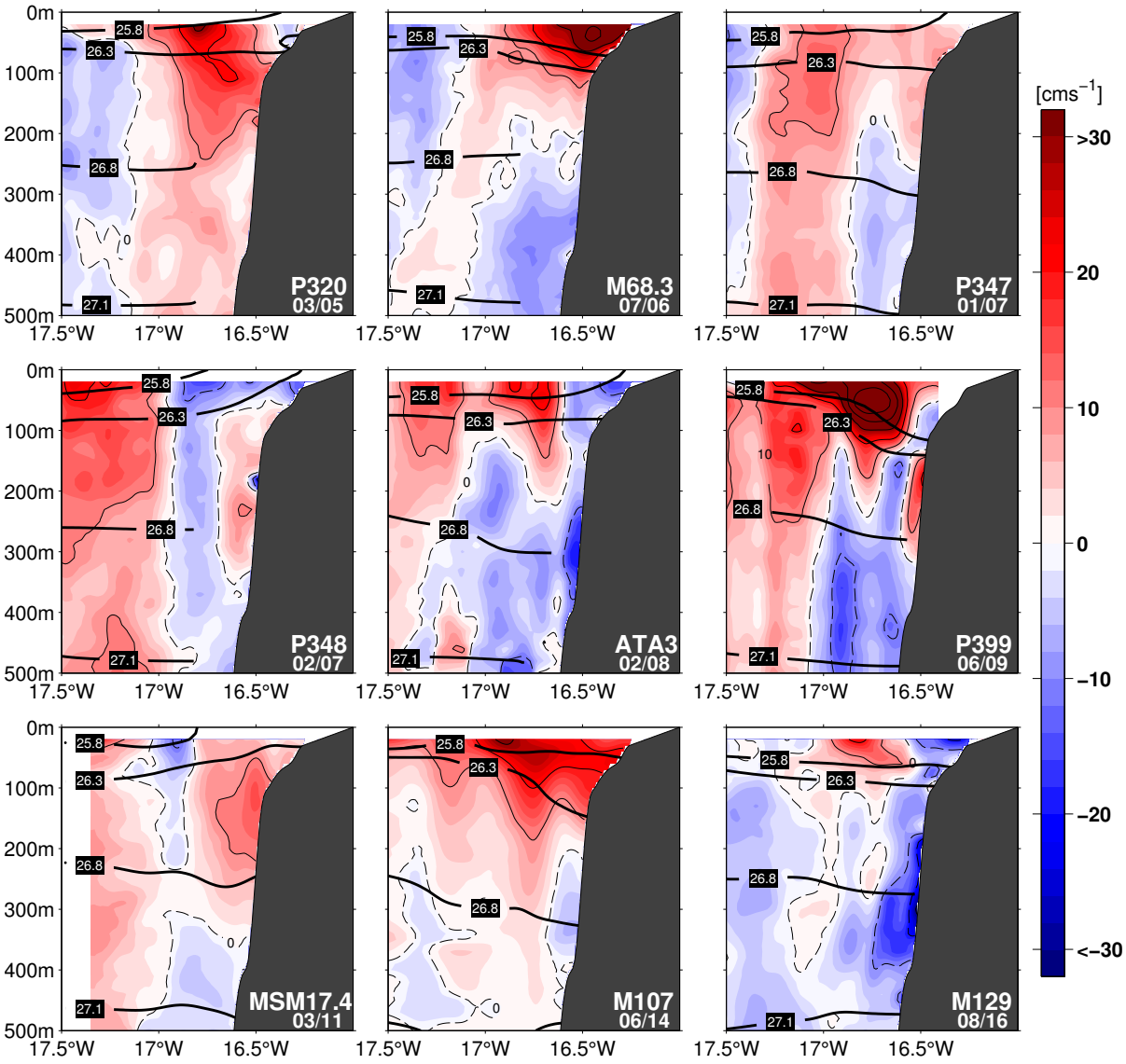

Figure 7: *Individual near-shore ship sections at 18°N of along-shore velocities* $[cms^{-1}]$ *in the surface and central water strata between 2005-2016. The cruise short as well as the month and year are given in the lower right corner of every subplot. Thick black contours depict potential density* (σ_Θ) *surfaces calculated from available CTD profiles along the sections. Thin black velocity contours are drawn in* $10cms^{-1}$ *increments for negative (dotted) and positive (solid) velocities. Positive values indicate northward velocities.*

observations.

The winter cruises are generally characterised by southward flow over the shelf, most pronounced during ATA3 with southward velocities below -$10cms^{-1}$ extending over the entire shelf. Northward velocities are weaker than during summer cruises, mostly confined to a core situated between 100m (MSM17/4) to 200m (P348) water depth, attached to the continental slope. The strongest northward velocities close to the slope and shelf

break during MSM17/4 are cleary confined to a core detached from the surface layer. The exception being P320, where the shape and speed of the currents resemble those observed during the summer cruises, with stronger northward velocities above 100m water depth and flow attached to the slope below. Still, weak southward velocities extend over parts of the shelf.

Southward velocities prevail in the lCW layer in most of the sections with the exception of P320, where no southward velocities in this layer observed. This feature seems most distinct during the summer cruises, especially *P399* and *M68/3* where southward velocities around -20cms^{-1} were observed and are distinctly separated from the northward flow in the uCW layer by the 26.8kgm^{-3}-isopycnal. Further offshore, i.e. more than 60km from the shelf break, the circulation varies significantly between individual cruises and doesn't seem to display any specific seasonality.

Coastal upwelling can clearly be seen in the seasonal shoaling and outcropping of the 25.8kgm^{-3}-isopycnal in the winter sections. The strongest upwelling signal can be seen during the P348 and MSM17/4 cruises. Here the 25.8kgm^{-3}-isopycnal outcrops furthest offshore, at around 16.8°W. The 26.3kgm^{-3}-isopycnal outcrops during P348, while during MSM17/4 it is at its second shallowest, at around 40-50m water depth over the shelf. Seasonal variability in the depth of the 26.8kgm^{-3}-isopycnal, namely the boundary separating the upper and lower central waters, is quite small. During MSM17/4 it can be seen dipping down following the core of the PUC.

Cruise short	Transport [Sv]	
	SW + uCW	lCW
P320	1.66	0
M68/3	1.45	-0.54
P347	0.79	-0.20
P348	0.26	-0.16
ATA3	0.62	-0.62
P399	2.10	-0.87
MSM17/4	0.80	-0.12
M107	1.86	-0.06
M129	0.33	-0.79
relaxation mean	1.77	-0.40
upwelling mean	0.66	-0.08

Table 3: *Mean north- and southward transport estimates ([Sv]) for individual cruises and for summer and winter seasons at 18°N from vmADCP measurements for the SW and uCW (σ_Θ <26.8), and lCW (26.8 < $\sigma_\Theta \leq$ 27.1) layers. For transport estimates, only positive/negative velocities were considered in the uCW+SW/lCW layers.*

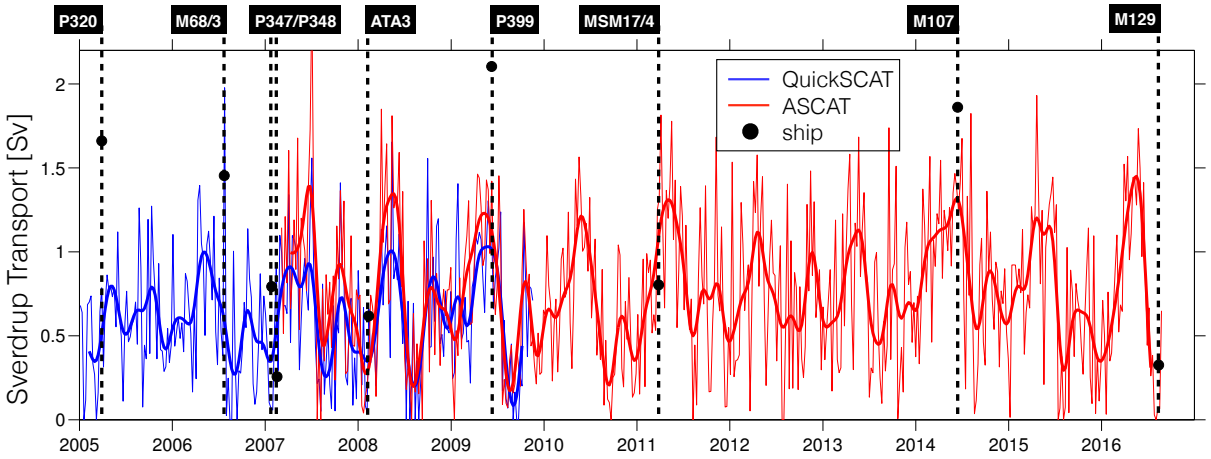

Figure 8: *Sverdrup transport ([Sv]) at 18°N, integrated from the eastern boundary to 17°W and calculated from weekly QuickSCAT (blue) and ASCAT (red) wind products as well as ship sections (black dots, cf Tab.3). Thin lines are weekly data, thick lines are three month lowpass filtered.*

Northward transports in the uCW and SW layers are generally higher during the summer cruises compared to the winter cruises (Tab.3). Note that velocities above 25m water depth are not resolved by the shipboard ADCP so large parts of the surface MC might not be captured and transports calculated from these sections might very well be underestimated. This is especially true for the summer cruises, when strongest surface currents related to the MC due to weak meridional wind stress are expected. The highest transport was observed during P399, where 2.10Sv were transported northward in a very defined core in the surface layer. Lowest transports of 0.26Sv were observed during P348. In the lCW layer the seasonal distinction is not quite as pronounced. However, generally larger southward transports are observed during summer cruises, with a maximum southward transport of -0.87Sv during P399 and no southward transport within the boundaries of integration during P320.

Sverdrup transport at 18°N calculated from satellite wind stress curl data (Fig.8) reflects the seasonal variability and semiannual cycle discussed previously, visible in the lowpass-filtered time series of both products. Towards the end of the upwelling season a sharp increase in transport is observed, followed by a sharp decrease. The secondary maximum around October-November is much more pronounced here than in the climatological wind stress curl data presented in the previous section. Interannual variability exists as well and while the decrease in northward transport is quite sharp from 1.5Sv o around 0.3Sv during the years 2008-2009 and especially 2016, the years 2012-2013 are characterised by a much lower seasonal variability. The wind stress curl is able to drive Sverdrup transport between 0-2Sv, of the same order as observed in the ship sections. Pronounced variability

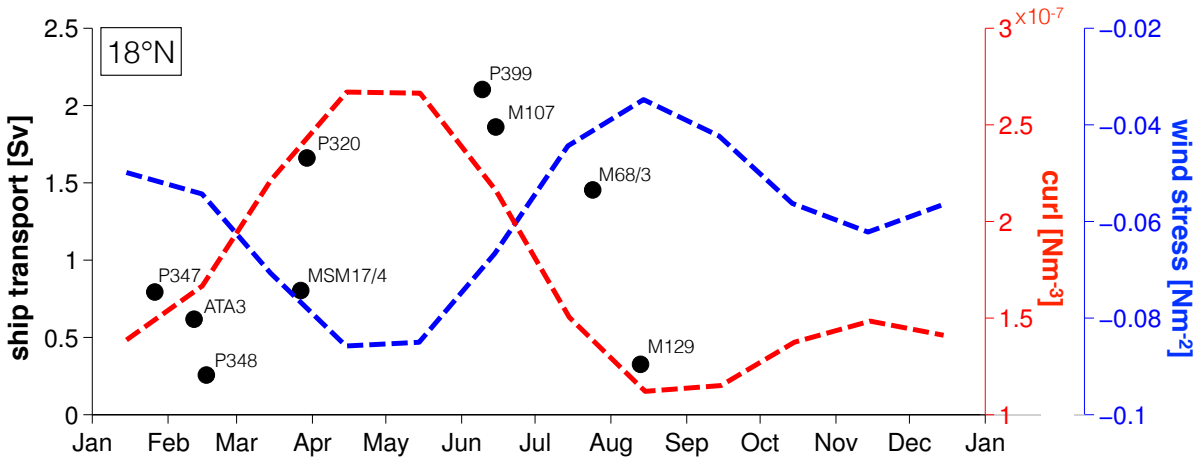

Figure 9: *SW + uCW (northward) transport estimates (cf. Tab.3) from individual cruises (black dots), seasonal wind stress curl from SCOW (red dotted line) and seasonal meridional windstress (negative southward) from SCOW (blue dotted line) at 18°N.*

on timescales of a few weeks exists and short periods of alternating enhanced/reduced transports dominate the time series. The ship estimates generally agree quite well with the calculated transports from the satellite time series. Periods of enhanced/reduced transports in the lowpass-filtered time series coincide with high/low ship estimates, except for P320 in 2005, where Sverdrup transport is about half of that observed in the ship section. During M68/3 and M107 short periods of intensified transport are of the same magnitude as the observed transports in the ship sections. There seems to be a discrepancy in transports calculated from the two wind products. QuickSCAT underestimates Sverdrup transport with respect to ASCAT, as is apparent from the period from 2007-2010, where the two products overlap. Further, it needs to be pointed out that due to the missing wind stress data close to the coast the calculated wind stress curl and hence Sverdrup transports are likely underestimated.

The number of cruises and their distribution over a span of eight months allows for comparing the emerging seasonality of individual transports to the seasonality of wind stress curl and meridional wind stress at 18°N (Fig.9). In doing so the observations made during the individual cruises are separated into seasonal means. Cruises P320, P347, P348, ATA3 and MSM17/4 were carried out during or towards the end of the upwelling season, characterised by periods of increasing wind stress and curl. Northward transports in the SW and uCW layers during this period are generally low (below $1Sv$), except for P320. With enhanced northward transports during periods of strong curl and enhanced Sverdrup transport, M68/3, P399 and M107 should best represent boundary current conditions during the relaxation season, when wind stress is rapidly decreasing and surface warming in the region occurrs (see also Fig.4a). On the basis of these observations the

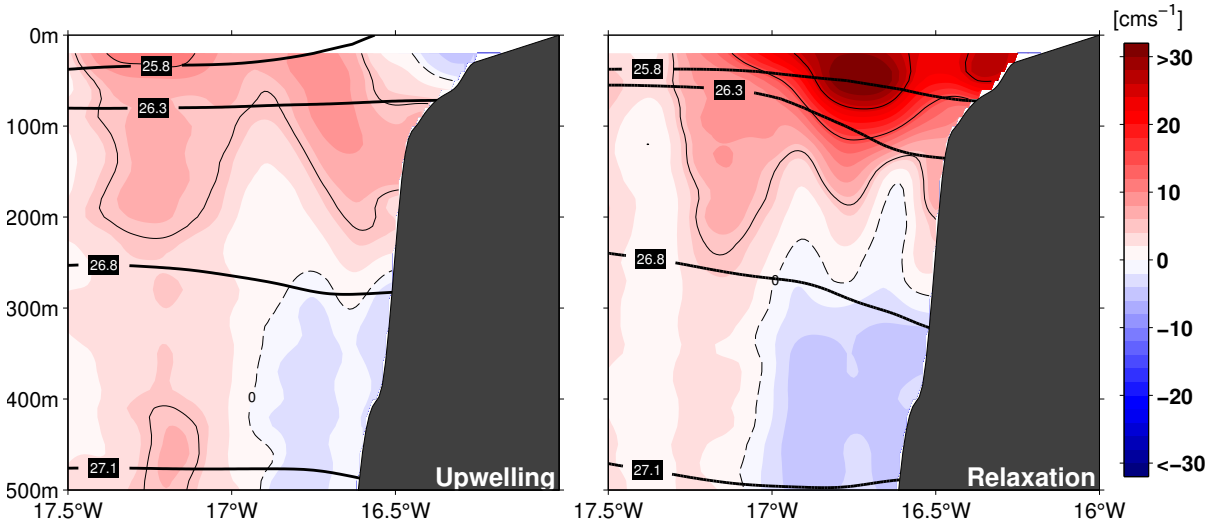

Figure 10: *Seasonal near-shore mean ship sections at 18°N of along-shore velocities* $[cms^{-1}]$ *in the surface and central water strata for upwelling (left panel) and relaxation (right panel) seasons. Thick black contours depict potential density* (σ_Θ) *surfaces calculated from available CTD profiles along the sections. Thin black velocity contours are drawn for* $5cms^{-1}$–$25cms^{-1}$ *in* $10cms^{-1}$ *increments. The dotted line depicts zero velocity. Positive values indicate northward velocities.*

eight cruises will therefore be divided into an *upwelling* and a *relaxation season* mean. M129 was carried out towards the end of the relaxation season and will therefore not be included in the relaxation season mean, also due to the weak circulation and transports observed during that cruise. Sverdrup transport during that time also shows very low values, following a sharp decrease.

We now focus on the seasonal mean sections along 18°N. The mean flow in the surface and upper uCW layers is strongest during the relaxation season with velocities over $20cms^{-1}$ extending offshore from the slope and over the continental shelf (Fig.10). Strong flows in the surface layer are likely associated with the surface MC or the surface manifestation of the PUC. Despite the high variability observed in the individual sections northward velocities are confined to a distinct maximum in the upper 150-200m. The two velocity cores stem from the strong velocities observed during M68/3 and especially P399. However, the general structure of the boundary circulation with the lower part of the current being attached to the shelf and the upper part extending offshore and upwards is discernable. Maximum southward velocities in the lCW layer in this mean section are not confined to a distinct core, however, southward velocities between 6-8cms^{-1} can be seen attached to the slope between 300m and 500m water depth with a width of about $50km$. The distinction of the two current regimes in the upper and lower central water layers separated by the $26.8kgm^{-3}$-isopycnal is much clearer in the seasonal sections.

During the upwelling season northward flow over the continental slope seems to be situated deeper in the water column compared to the summer months and maximum velocities are lower (less than $15 cms^{-1}$). It seems as if northward flow above $10 cms^{-1}$ is permanently attached to the shelf break at around 100m depth during both seasons, being deflected further offshore by southward velocities over the shelf during the upwelling season. The likely cause for southward velocities over the continental shelf is a geostrophic response to upwelling. The $26.8 kgm^{-3}$-isopycnal again clearly separates northward flow in the uCW layer from weaker southward flow in the lCW layer during this season.

Boundary circulation transport during the relaxation season is almost three times higher in the SW and uCW layers compared to the upwelling season ($1.77 Sv$ and $0.66 Sv$, respectively) and five times higher in the lCW layer (-$0.40 Sv$ and -$0.08 Sv$, respectively, see also Tab.3). The depth of both the $26.8 kgm^{-3}$ and $27.1 kgm^{-3}$-isopycnals at 18°N is rather invariant between the two seasons, while the upwelling signal can be clearly seen in the variability of the $25.8 kgm^{-3}$-isopycnal and even though less pronounced, the $26.3 kgm^{-3}$-isopycnal (Fig. 10).

4.2 Hydrography and Water Mass Characteristics

The observed hydrographic conditions along 18°N and its seasonal variability will first be presented for individual cruises, followed by a description the relative contributions of South and North Atlantic central waters through water mass analysis on the basis of these observations. A look at seasonal mean sections of salinity, temperature and associated water mass distribution will highlight the role of the seasonal mean circulation described in the previous section. The meridional variability is described using seasonal mean property-property plots along the coast in the study region.

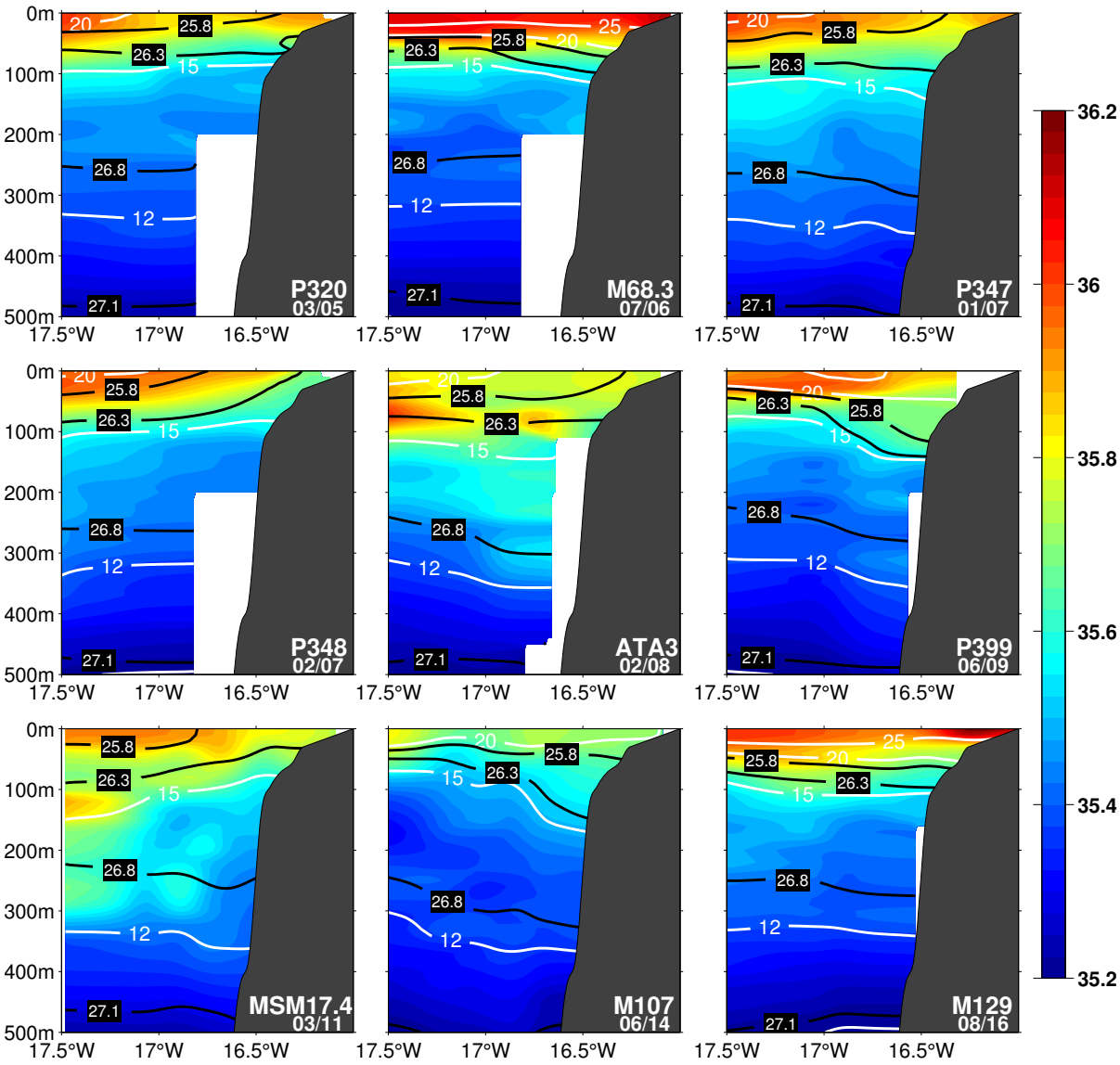

Figure 11: *Individual sections of salinity along 18°N from CTD sections during the nine cruises. Thick black contours depict potential density (σ_Θ) surfaces calculated from available CTD profiles along the sections. White lines depict isotherms.*

The hydrographic sections during the individual cruises highlight the seasonal differences related to coastal upwelling in the nearshore region above 100-150m (Fig.11). While the summer cruises are generally characterised by warm temperatures in the surface layers and over the shelf (above $25°C$ during M68/3 and M129 and above $20°C$ during P399 and M107) temperatures during the winter cruises are significantly colder (lower than $20°C$ in the surface layer and close to $15°C$ over the shelf during P348 and MSM17/4). The $20°C$ isotherm outcrops away from the shelf region westwards of 17°W during all winter cruises. Salinities are generally higher close to the surface associated with the TSW

Waters in the uCW layer generally show lower salinties during the summer cruises, most pronounced during M107 and M129. However, fresher waters can be seen close to the slope during P348 and MSM17/4, likely associated with positive velocities in that same depth range (cf. Fig7). Unfortunately, during P320, M68/3, P348 and ATA3 CTD measurements in the vicinity of the slope in the lower uCW and lCW are missing. Possible hydrographic changes connected to north- as well as southward currents in that region cannot be discussed. The central water layer is prone to intrusions of waters of higher/lower salinities compared to its surrounding waters due to the potential density properties of North and South Atlantic central waters. Examples of these intrusions are clearly visible in the upper uCW layer (around or just below the $26.3 kgm^{-3}$-isopycnal) during ATA3 and MSM17/4, where high salinity waters intrude into layers of predominantly fresher waters. On the other hand, low-salinity waters can be seen surrounded by higher salinity waters during the summer cruises M68/3 and M107 as well as winter cruises MSM17/4 and P347. Salinities during ATA3 are the highest observed in the uCW layer, possibly due to dominating southward velocities during that cruise.

Variability in the lCW layer is less pronounced, however, higher salinities close to the slope between 300-500m water depth during P399 could be related to enhanced southward flow in that layer. Changes of high and low salinity waters seem to be confined to the upper lCW layer. The low-salinity waters below the $27.1 kgm^{-3}$-isopycnal close to 500m water depth belong to the AAIW. The boundary between the central water masses and the AAIW seems to be rather invariant between individual cruises of either season. The most noticable change is a deepening of the $27.1 kgm^{-3}$-isopycnal coinciding with northward velocities in the lCW layer during M107.

The overall freshening observed in the uCW layer, and to a lesser extent also in the lCW layer, from the upwelling to the relaxation season coincides with a cooling of the water masses as well (Fig.12). This can be best seen in the shoaling of the $13°C$- and $14°C$-isotherms in the uCW layer as well as the $12°C$-isotherm in the lCW layer in the relaxation season mean. This fact further confirms a larger import of central waters of

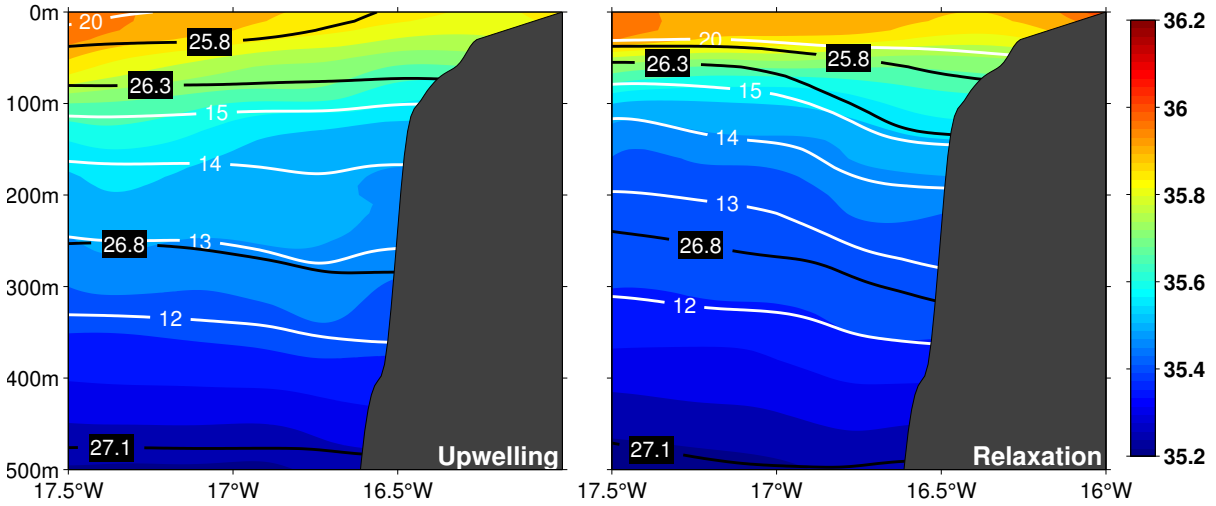

Figure 12: *Seasonal near-shore mean ship sections at 18°N of salinity in the central water stratum for upwelling (left panel) and relaxation (right panel) seasons. Thick black contours depict potential density (σ_Θ) surfaces calculated from available CTD profiles along the sections. White contours depict isotherms.*

South Atlantic origin during the relaxation season compared to the upwelling season. The difference in temperature of two water parcels of predominantly South/North Atlantic origin exhibiting the same potential density can be as high as 2-3°C (see also Fig.2).

Looking at the water mass characteristics calculated from the observed temperature and salinity sections during the individual cruises further underlines the seasonal variability of hydrographic properties, their origin, as well as its connection to the boundary circulation (Fig.13). However, one fact that is more clearly accessible when looking at water mass concentrations and opens up a new interpretation of the results so far is an apparant change of water mass characteristics within the central water stratum. Water mass concentrations change drastically when going from the uCW to the lCW layers, observed during all cruises in the data set. Concentrations generally exceed 70-80% throughout most of the uCW layer and can as high as 90% close to the shelf break, while decreasing to values lower than 50-60% in the lCW layer below. During the two summer cruises P399 and M107 higher SACW concentrations reach into the upper lCW layer. The 70%-isoline appears to be following the 26.8kgm^{-3}-isopycnal, most pronounced during cruises P320, M68/3, P399 and M129. Intrusions, that were observed as higher salinites compared to ambient waters during MSM17/4, can now be attributed to waters of North Atlantic origin, with SACW concentrations below 20%, i.e. NACW concentrations above 80%. Further, the lower SACW concentrations between 40-60% in the lCW layer point towards a mixture of water masses with South and North Atlantic origin and hence a longer residence time of an older water mass. High SACW concentrations would therefore

correspond to a more recent renewal of waters in the uCW layer in the boundary currents during the relaxation season.

The observed water mass concentrations also reflect the current observations of the individual cruises. The high SACW concentrations attached to the continental slope at a depth around 100m during MSM17/4 resemble the shape and location of the northward current during the cruise. Highest concentrations of SACW properties are observed during M107, with SACW characteristics above 85% throughout almost all of the uCW

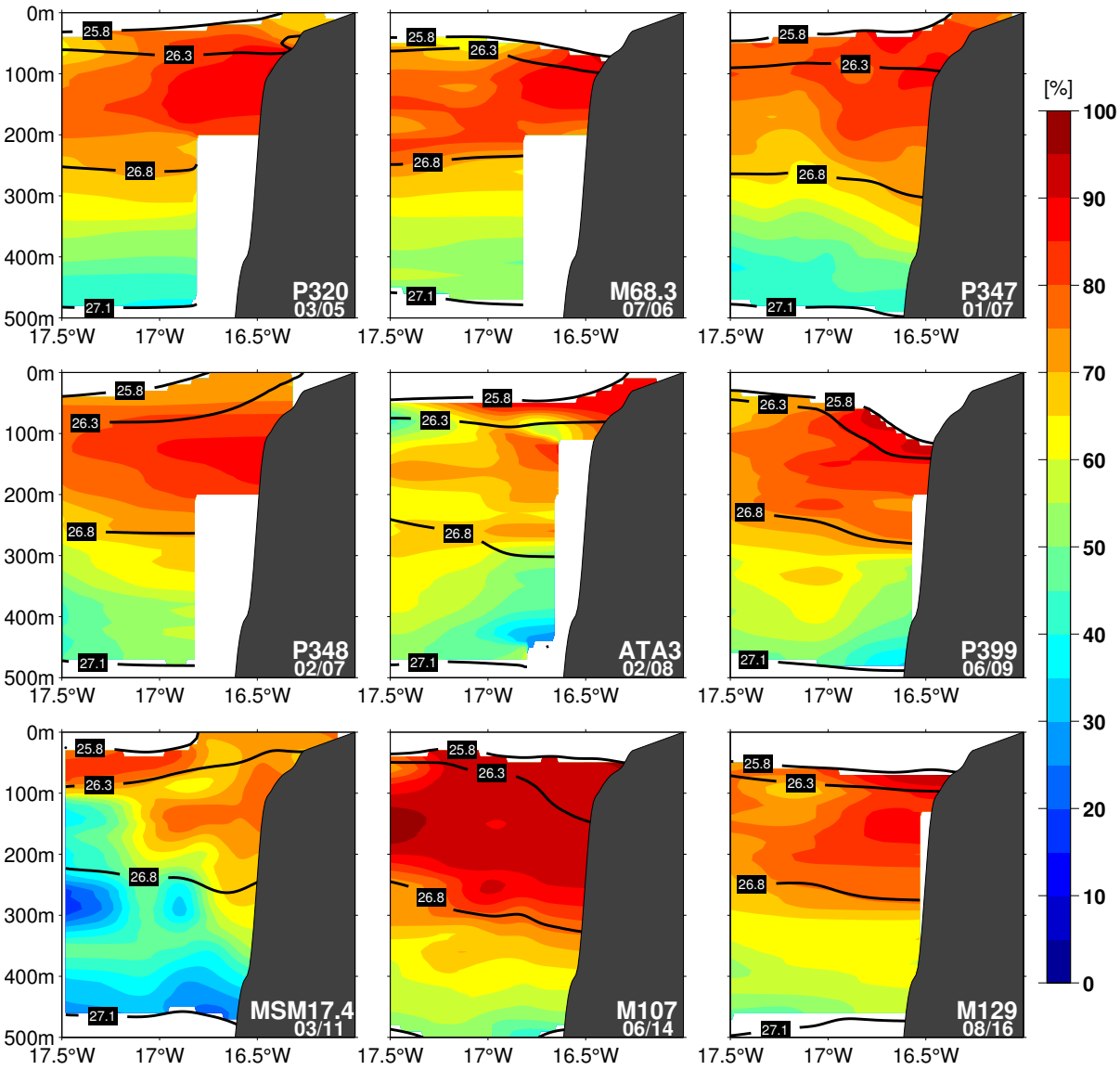

Figure 13: *Individual sections of SACW concentrations along 18°N from CTD sections during the nine cruises. 100% (red) is pure SACW and 0% (dark blue) is pure NACW. Thick black contours depict potential density (σ_Θ) surfaces calculated from available CTD profiles along the sections*

layer, associated with northward velocities extending over the same area.

Lowest SACW concentrations in the lCW layer close to the continental slope during cruises ATA3 and MSM17/4 seem to be associated with southward currents in that layer. Despite the absence or rather the lack of observation of a distinct PUC core during M129, SACW concentrations at and below the shelf break are high (above 80%). This suggests that a PUC had been there, but seized before the observations were made, highlighting the strong variability in the region and corresponding well to the sharp decrease of Sverdrup transport prior to the observations mentioned in the previous section.

Upwelled waters over the shelf during the winter cruises (upwelling season) consist of central waters of predominantly South Atlantic origin, being fed by waters close to the shelf break where highest SACW concentrations are found during the upwelling season. Concentrations above 70% are observed over the shelf (Figs.13,14). Due to the biogeochemical properties of SACW this has implications for the nutrient supply during the upwelling season compared to regions fed by mostly NACW, to be discussed later on. The clear distinction in uCW and lCW SACW concentrations in both the upwelling and the relaxation season agrees well with the southward velocities in the lCW layer.

Waters in the uCW layer at 18°N seem to be renewed through advection of SACW from the south in the boundary circulation. Judging from the mean circulation as well as the large amounts of water with SACW concentrations above 80% in the uCW layer this renewal seems to happen mostly during the relaxation season. The lCW layer does not

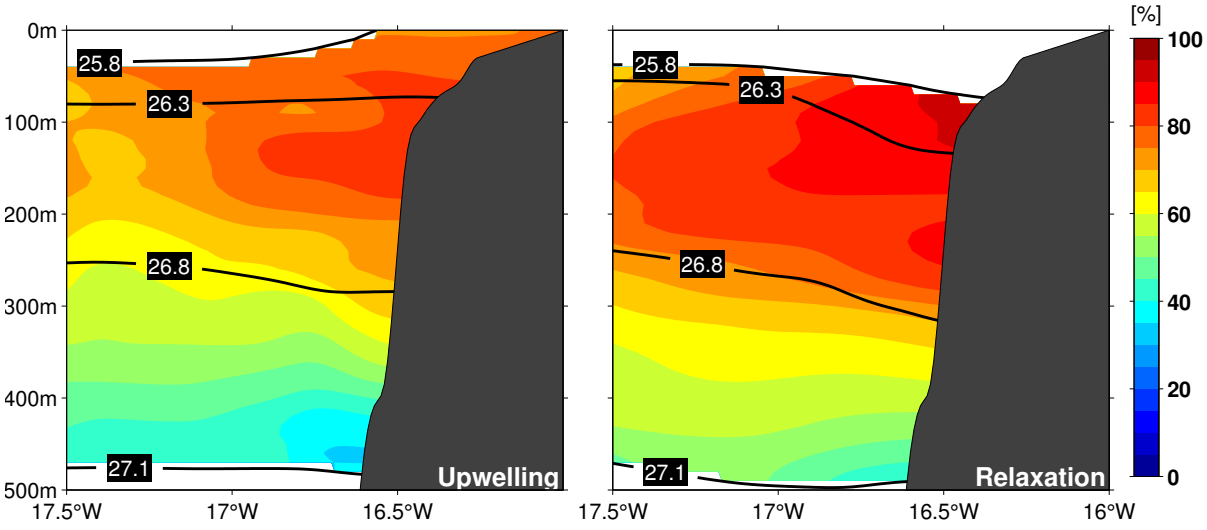

Figure 14: *Seasonal near-shore mean ship sections at 18°N of SACW concentrations in the central water stratum for upwelling (left panel) and relaxation (right panel) seasons. Thick black contours depict potential density (σ_Θ) surfaces calculated from available CTD profiles along the sections.*

seem to experience this kind of renewal from the south. Occasionally though central waters of North Atlantic origin seem to penetrate this layer close to the slope from the north as well. To further analyse this water mass renewal, first a closer look at the water mass distribution in the MUR from climatological data will be presented.

The climatological distribution of central waters in the MUR between 14°N - 21°N is generally characterised by a north-south shift in source waters that make up the central water stratum. Central waters of predominantly South Atlantic origin are dominating in the south, while warmer and more saline NACW are found in the north (Fig.15a). However, due to the seasonal variability of the boundary circulation described in the previous section and the associated water mass changes that go along with them, a seasonal, meridional dependency is expected. This fact is also apparent when analysing the climatological mean salinity in the boundary current regime (between the coast and 100km offshore) in MIMOC (Fig.15b). With the beginning of the relaxation season we see a distinct freshening in the northern part of the MUR, also apparant in the northward intrusion of high SACW concentrations during that period. The same freshening was

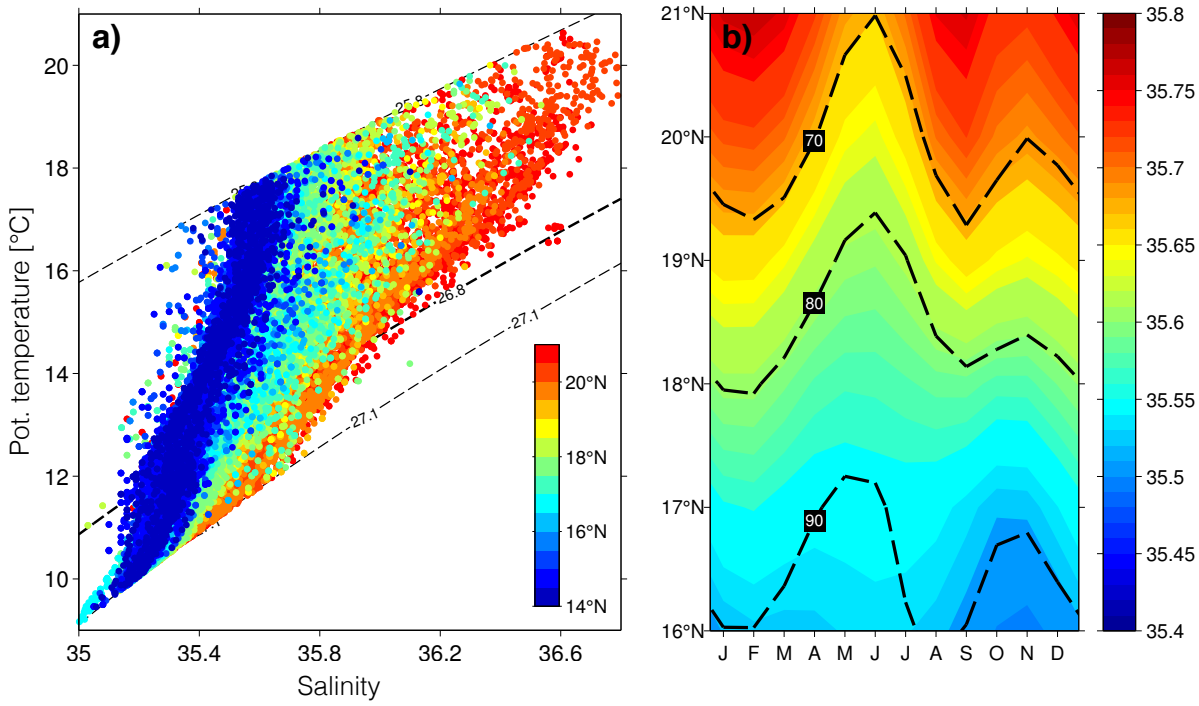

Figure 15: *(a) Potential temperature against salinity diagram in the central water stratum from MIMOC. Dots are colored according to their latitude. Thin dotted lines define the upper and lower boundaries of the central water stratum. The thick dotted line represents the boundary between upper and lower central waters. (b) Mean salinity in the upper central water layer 100km offshore between 16°N - 21°N. Black dotted lines depict SACW concentrations.*

observed in individual cruise sections as well as in the mean for the relaxation season at 18°N. A secondary peak is visible during October-November. In general, the seasonal cycle in salinity between 18°-20°N resembles that of the wind stress curl and Sverdrup transport at the same latitudes. To further analyse this relationship and to see whether this fact is supported in the hydrographic cruise data north of the previously presented sections as well, property-property diagrams of potential temperature and salinity as well as SACW concentrations within the central water stratum are analysed in a 100km wide band along the coast.

The freshening and associated cooling in the uCW layer during the relaxation season observed at and around 18°N is also observed further to the north (Fig.16a,c,e). A slight shift towards more saline waters during both seasons can be seen from the south to the north. This points to generally higher SACW concentrations in the south (see also Fig.15a) and a mixing of SACW with the surrounding waters of higher NACW content. However, the seasonal differences in salinity on isopycnals are large at all latitudes. The effect of the inflow of SACW within the boundary currents acting to renew central waters in the uCW layer seems to be most noticable at higher latitudes. The seasonal differences between 17°-18°N are mostly confined to the upper uCW layer while further north and especially north of 19°N the seasonal differences become larger in the lower part of the uCW layer as well. In the lCW layer the seasonal differences are negligible as the summer curve nears the winter curve. Moving northward along the coast a slight shift towards lower SACW concentrations in both seasons can be seen in this layer, again pointing towards a possible northerly pathway for NACW in the lCW layer. The variability between measurements of individual cruises from both seasons (indicated by ± 1 standard deviation) is relatively small in the lCW layer, while in the uCW variabilty is generally higher, especially during winter. This points to a relatively homogeneous water mass consisting of almost equal parts SACW and NACW, with SACW concentrations between 40-60% (Fig.16b,d,f).

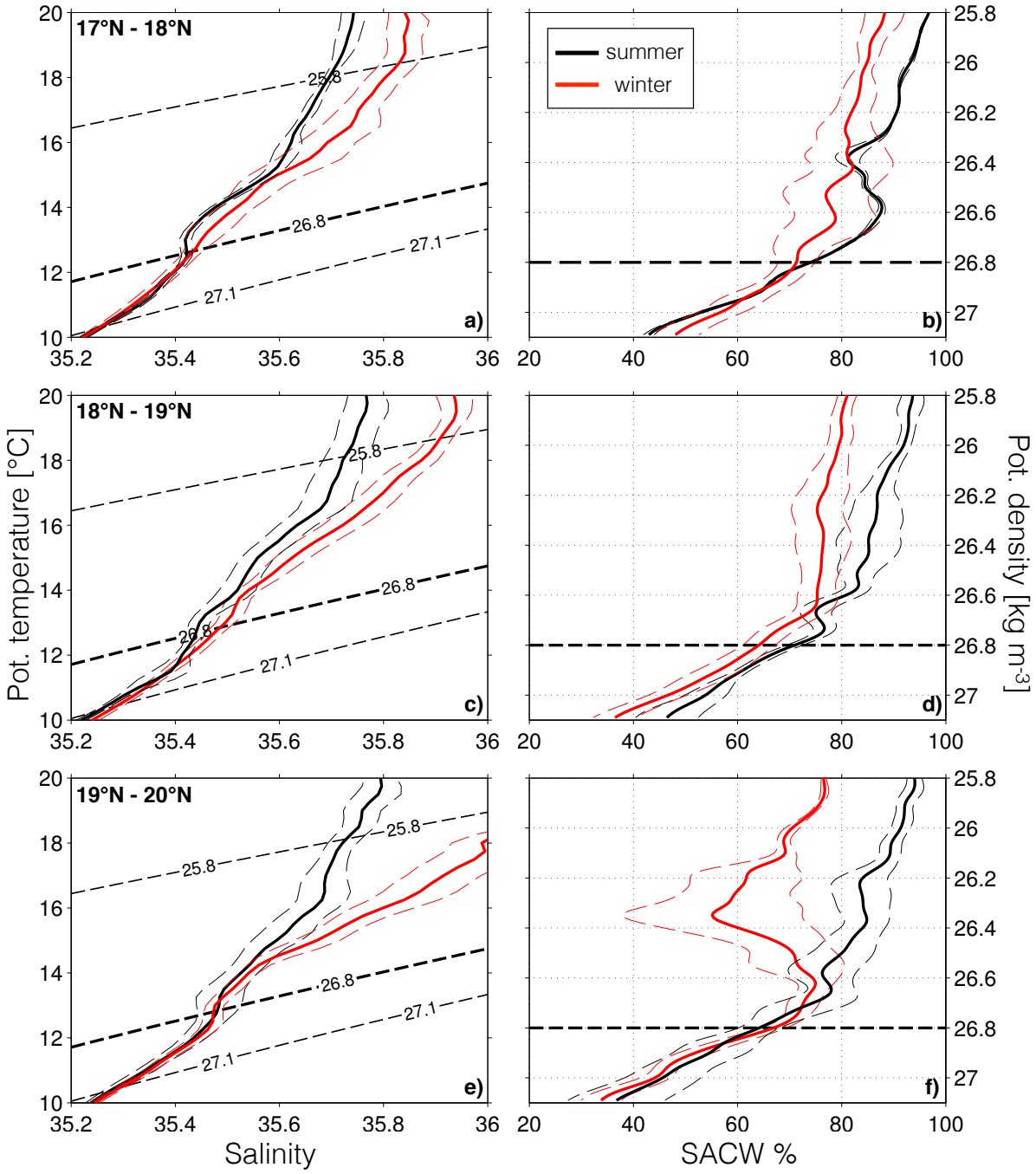

Figure 16: *Seasonal mean property-property plots in a band 100km (the western integration boundary of the boundary currents) from the coast at different latitudes around the shallow OMZ. (a,c,e) Potential temperature against salinity and (b,d,f) potential density against SACW content for summer (black) and winter (red) cruises. Thin dashed lines represent ±1 standard deviation. The 26.8kgm^{-3}-isopycnal (thick black dashed line in all panels) represents the boundary between upper and lower central water layers.*

4.3 Oxygen Distribution

The oxygen concentrations observed in the central water layer during the individual cruises will be described in this subsection. Measurements made during P320 had to be excluded due to faulty data. Judging from the current observations and the hydrographic properties observed throughout the cruises described in the previous sections, one would expect oxygen concentrations to vary seasonally as well.

The climatological oxygen distribution in the MUR (Fig.17) shows minimum oxygen concentrations above 200m water depth (representative of the shallow oxygen minimum) below $60 \mu molkg^{-1}$ centered just north of 18°N at a water depth between 100-110m. Higher minimum oxygen concentrations are found to the north and to the south. Higher concentrations in the north highlight the influence of waters of the subtropical gyre, which are higher in oxygen due to a more recent ventilation.

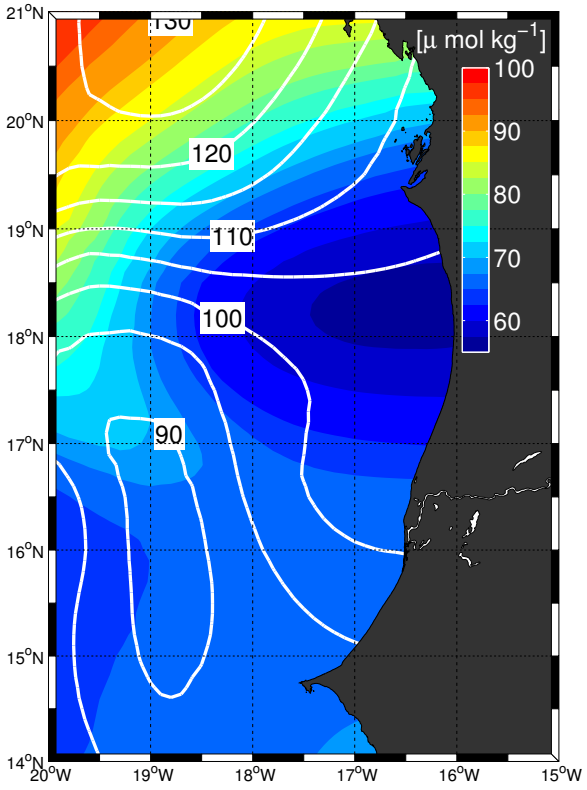

Figure 17: *Climatological minimum oxygen concentrations above 200m water depth from MIMOC. White contour lines depict climatological depth of oxygen minimum.*

Oxygen concentrations observed throughout the eight cruises exhibit pronounced variability in both central water layers. Observed oxygen concentrations in the uCW layer are generally higher than in the underlying lCW layer throughout all cruises (Fig.18), in agreement with the currents and hydrographic properties described in previous sections. The advection of SACW waters during the relaxation season seems to ventilate that layer and transport waters depleted of oxygen during the upwelling season northward. In the lCW layer, the water masses with mixed SACW/NACW properties and weak southward currents agree well with the low oxygen concentrations there. However, individual events point towards a high variability in oxygen concentrations. During P347 oxygen concentrations in the lCW layer are notiably higher than during M68/3 which was carried out just six months prior. The lower SACW concentrations point towards an advection of oxygen-richer NACW from the north. The same is clearly visible between 300-400m

water depth close to the slope during ATA3, where southward velocities coincide with low SACW concentrations and higher oxygen concentrations. These might only be intermittent features rather than represent a constant northerly supply of oxygen-richer NACW but they seem to form a ventilation pathway in the lCW layers from the north. Westerly intrusions in the uCW as well as the lCW layer during MSM17/4 were previously shown to be consisting of central water of North Atlantic origin and have higher oxygen concentrations above $70 \mu molkg^{-1}$ compared to their surrounding waters.

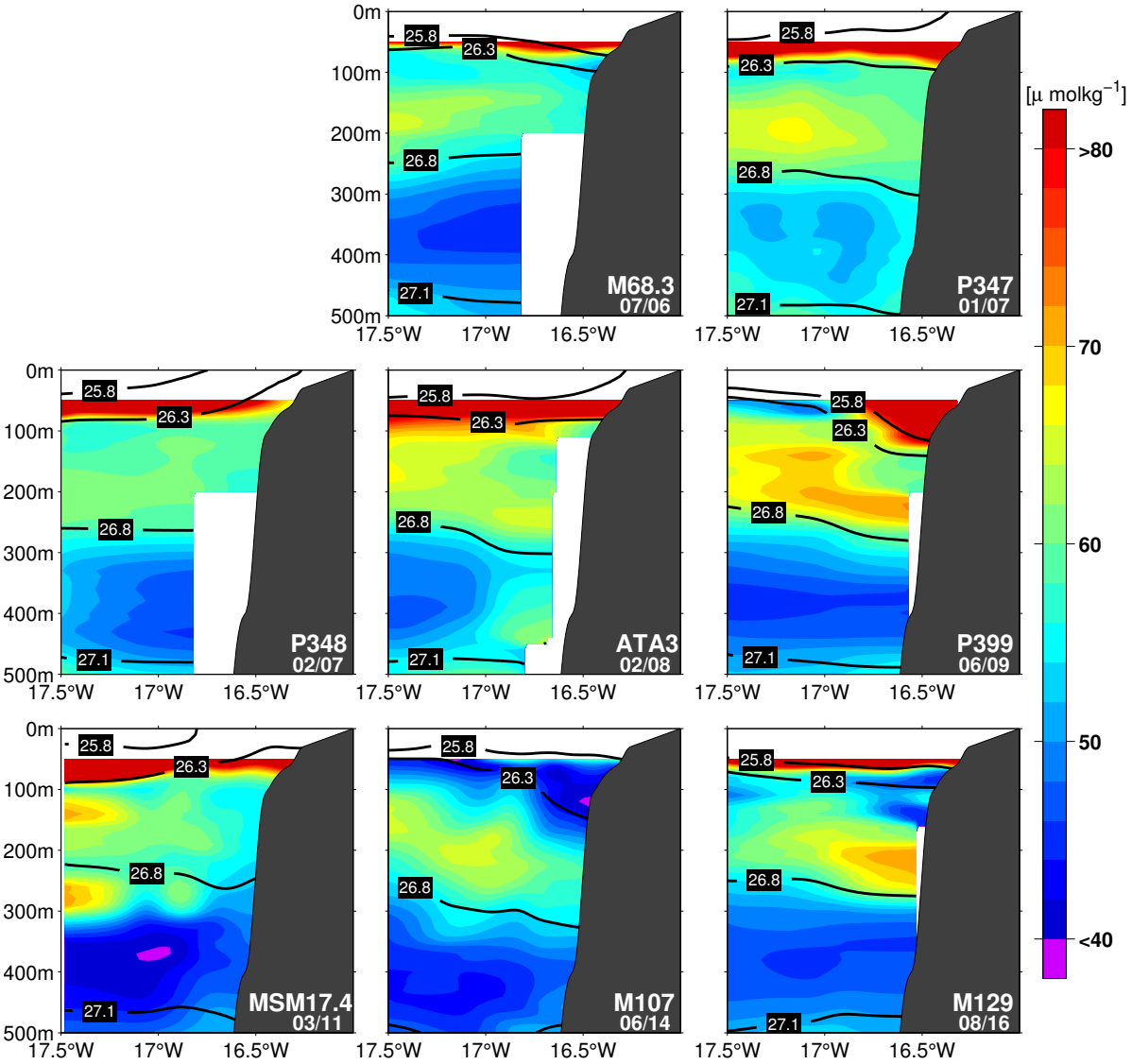

Figure 18: *Individual sections of oxygen concentrations in* $[\mu molkg^{-1}]$ *along 18°N from CTD sections during the nine cruises. Oxygen values above 50m water depth are excluded, as were oxygen measurements from the P320 cruise. Thick black contours depict potential density* (σ_Θ) *surfaces calculated from available CTD profiles along the sections*

Despite the large inflow of SACW coinciding with enhanced oxygen concentrations throughout most of the uCW layer, lowest oxygen concentrations are observed around the shelf break during the summer cruises, especially M107 and M129. Very low oxygen concentrations slightly above $40 \mu molkg^{-1}$ are observed laterally extending between the $25.8 kgm^{-3}$ and $26.3 kgm^{-3}$-isopycnals around 100m water depth. The strong observed velocities during M107 lead not only to a large inflow of high-SACW characteristic waters but also lead to enhanced mesoscalar activity, increasing isopycnal mixing and transporting waters low in oxygen away from the shelf break. Very high oxygen concentrations associated with strong northward currents were abserved during P399. However, these are confined to the SW layer and are most likely associated with the MC current rather than an advection of SACW in the PUC. Just below the $26.3 kgm^{-3}$-isopycnal, displaced by the large northward velocity core, lowest oxygen concentrations attached to the slope are found. Offshore, minimum oxygen concentrations around the $26.3 kgm^{-3}$-isopycnal resemble conditions observed during the other summer cruises. Below the shallow oxygen minimum observed during the summer cruises, oxygen concentrations increase again to maximum oxygen cncentrations ad middepth around 200-250m depth.

Oxygen concentrations between the $25.8 kgm^{-3}$ and the $26.3 kgm^{-3}$-isopycnals during the winter (upwelling) cruises are highly enhanced, pointing towards a direct ventilation through the outcropping of the isopycnals and/or diapycnal supply enhanced during the winter season.

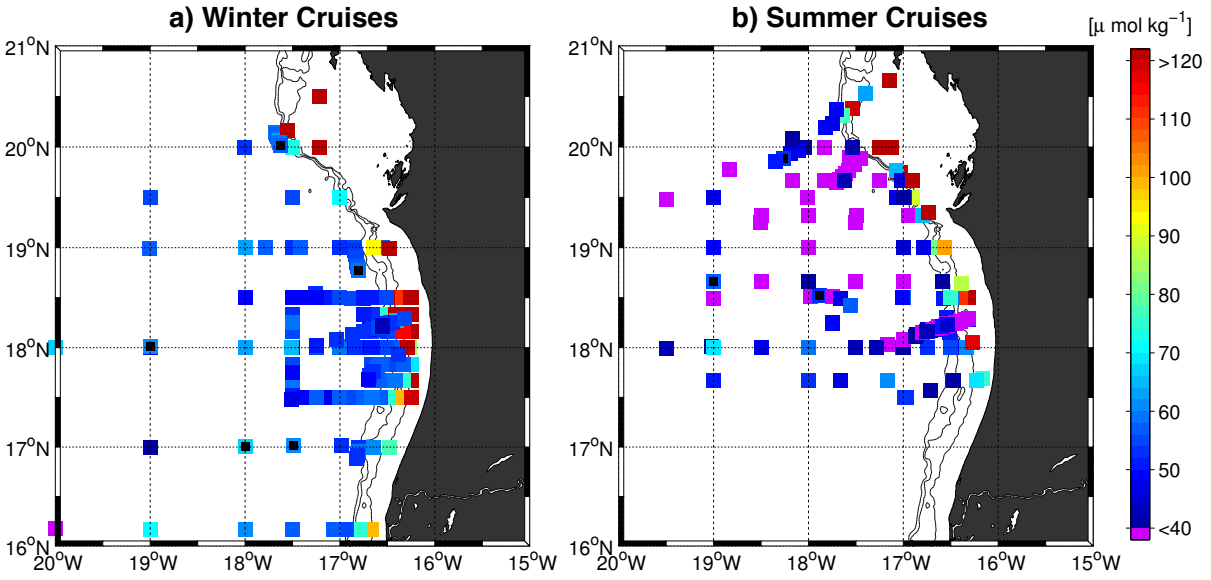

Figure 19: *Minimum oxygen concentration above 200m water depth representing the shallow oxygen minimum for (a) winter and (b) summer cruises. Thin black contours depict the 50m, 100m and 200m isobaths. Oxygen concentrations below 40 $\mu molkg^{-1}$ are marked in purple.*

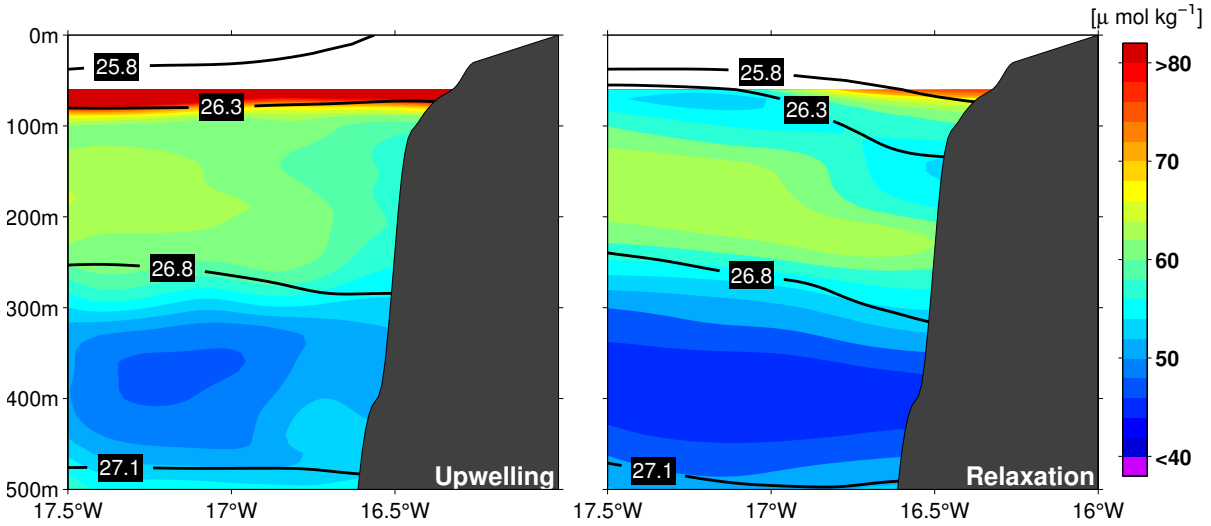

Figure 20: *Seasonal near-shore mean ship sections at 18°N of oxygen concentrations in the central water stratum for winter (left panel) and summer (right panel) cruises. P320 is excluded from the mean. Values above 50m water depth are excluded. Thick black contours depict potential density (σ_Θ) surfaces calculated from available CTD profiles along the sections. Thin black velocity contours are drawn.*

In the uCW layer oxygen concentrations generally decrease towards the slope during winter and summer cruises. However, in the lCW layer, oxygen concentrations increase towards the slope. These higher oxygen concentrations close to the deep oxygen minimum, are associated with high NACW concentrations and southward velocities, pointing to a possible ventilation mechanism during boreal winter when the CVFZ is at its southernmost position. Northward flow extending partly into the lCW layer during e.g. MSM17/4 seems to lead to lower oxygen concentrations in the lower uCW layer close to the $26.8 kgm^{-3}$-isopycnal.

Low oxygen concentrations (below $40 \mu molkg^{-1}$) can be traced as far away as 250km from the shelf break during the summer cruises (Fig.19b). They are following the depth contours around the shelf break and are most pronounced during M107 and M129 (see also Fig.18). Lowest oxygen concentrations observed during the winter cruises generally do not fall below $40 \mu molkg^{-1}$, even though the location of the isopycnals point to upwelling during all of them. The low concentrations around 100m depth during the summer cruises are therefore likely associated with enhanced remineralisation due to prolonged high productivity in the surface layers offshore after the upwelling season. Additionally, since oxygen concentrations are lowest close to and extending laterally along isopycnal surfaces offshore from the shelf break (Fig.18,20), isopycnal mixing enhanced by mesoscale processes connected to seasonally strengthened near-surface currents likely acts to advect water from the coast into the offshore region.

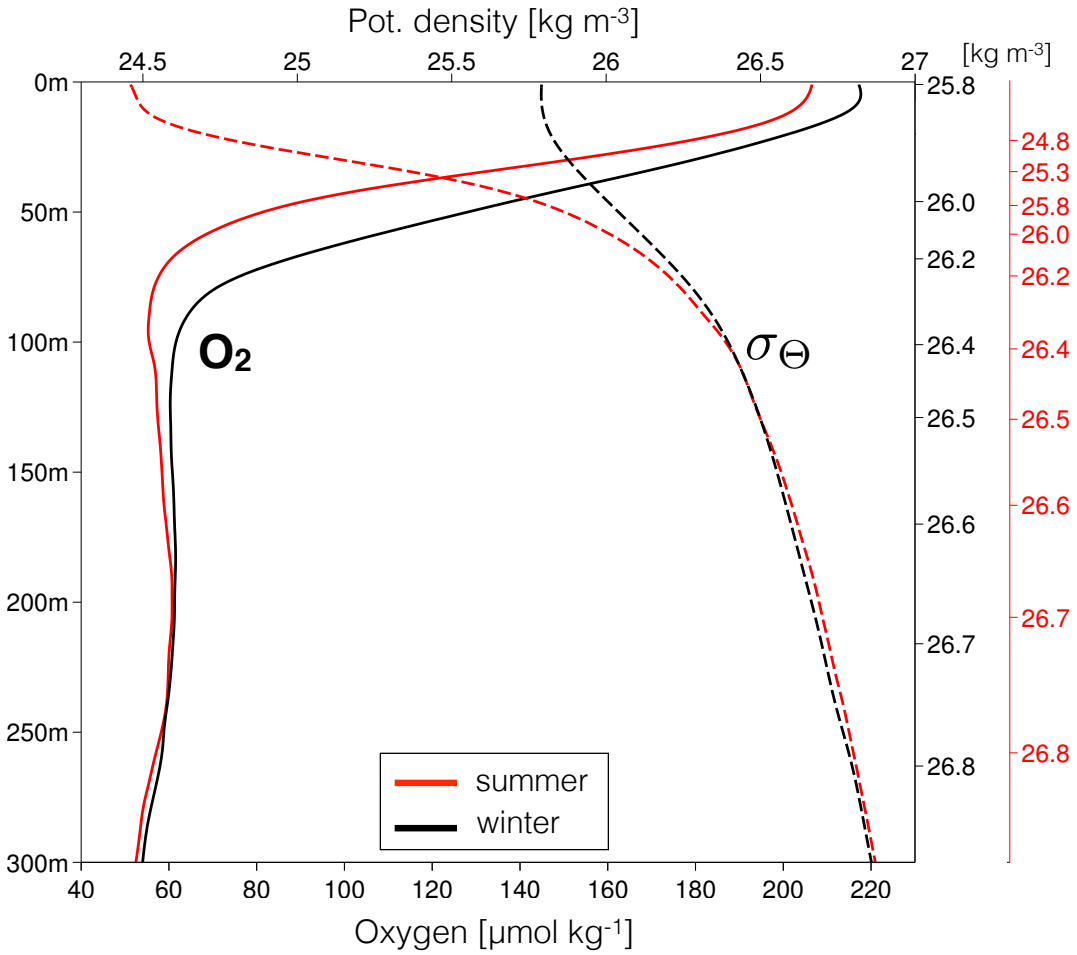

Figure 21: *Seasonal mean oxygen concentration (solid lines) and potential density (dashed line) for summer (red) and winter (black) cruises in the region of the shallow oxygen minimum (cf. Fig.17). Left hand side y-axis depicts depth space, black and red y-axes on the right hand side depict potential density space for winter (black axis) and summer (red axis) means, respectively.*

Looking at the mean oxygen concentrations in the region of the shallow OMZ down to 300m water depth (roughly coinciding with the boundary between the upper and lower central waters), a possible connection of the seasonally varying minimum oxygen concentrations of the shallow OMZ and the stratification becomes apparent. The structure of the two averaged oxygen profiles is similar during both seasons (Fig.21). The oxycline (i.e. the region where oxygen decreases most rapidly with depth) separates oxygnated (above $200 \mu molkg^{-1}$) waters at the surface from a shallow oxygen minimum around 100m water depth. Below concentrations increase towards an oxygen maximum with oxygen concentrations slightly higher than the minimum. The deep oxycline separates this maximum from the deep oxygen minimum around 400m depth (not shown).
The oxycline is much shallower during the summer cruises than during the winter cruises.

This coincides with a much more defined pycnocline and enhanced stratification. During the winter cruises, stratification is greatly reduced due to coastal upwelling and the upwelled central waters extending far offshore. Minimum oxygen concentrations are reached at greater depths compared to the summer cruises and in combination with the reduced stratification this points to a supply of oxygen from the surface layers into the shallow OMZ during the upwelling season, therefore reducing the oxygen gradient in the water column.

4.4 Meridional Penetration of Water Mass Characteristics

The northward penetration of SACW in the boundary currents in the uCW layer as well as the southward penetration NACW in the lCW below is shown exemplary along two meridional sections along the coast for cruises M68/3 and P347. These two cruises are chosen, because they *(i)* provide the most extensive and uniform meridional as well as zonal coverage and *(ii)* are the only two cruises in the data set that were conducted in successive relaxation/upwelling seasons. Additionally, oxygen concentrations in the central water stratum are shown. Available CTD-O_2 stations between 17°-20°N from the two cruises are averaged within two bands along the coast. The near-shore band includes all CTD-O_2 measurements down to 500m water depth taken within 100km from the coast. This boundary was chosen to coincide with the integration boundaries for transport calculations in the boundary currents. The offshore band includes stations sampled between 100-200km from the coast.

First, it is worth discussing the meridional change in the depth of the central water boundaries. The meridional change in the upper boundary of the central water stratum undergoes little change throughout both sections and both seasons. However, during M68/3 the thickness of the uCW layer is decreasing moving northward along the coast. A sharp upward sloping of the $26.8 kgm^{-3}$-isopycnal can be seen just north of 18°N. This is possibly connected to the relatively strong southward velocities at the same latitude during M68/3 observed below 250m water depth leading to a thickening of the lCW layer. In the offshore section the amount of NACW intruding southward into the lCW layer is even higher while in the uCW layer largest SACW concentrations extend only to about 18°N. This suggests that advection of purer SACW northward is restricted to the boundary currents. The depth of the lower boundary of the lCW shoals meridionally during both cruises, from 490m to 430m along the offshore section during M68/3, seemingly following the $26.8 kgm^{-3}$-isopycnal. Generally it can be said that in the near-shore section a thick uCW layer comes with an thin lCW layer and vice versa, pointing to a baroclinic response.

While these meridional sections also show small scale intrusions, as shown in previous sections, the main focus in these figures should be on the general structure caused by the aforementioned different circulations in the upper and lower central water layers. The southward intrusions of waters consisting of predominantly NACW in the lCW layer and the northward penetration of high SACW concentration in the uCW layer reflect the different circulation cells during both cruises.

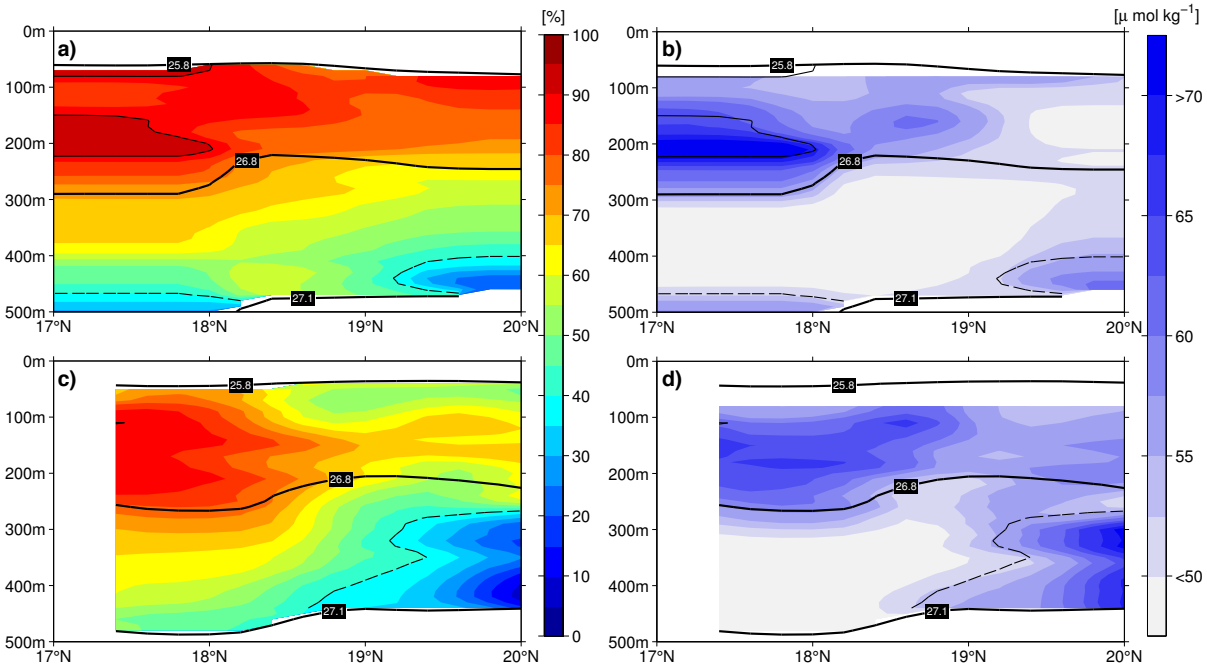

Figure 22: *Meridional water mass and oxygen distributions for (a,b) near-shore and (c,d) off-shore bands during M68/3. 100% represents pure SACW, 0% pure NACW. The thick black contour lines in all panels depict the potential density boundaries of the central water stratum. Thin solid and dashed black lines indicate the 90% and 40% isolines, respectively.*

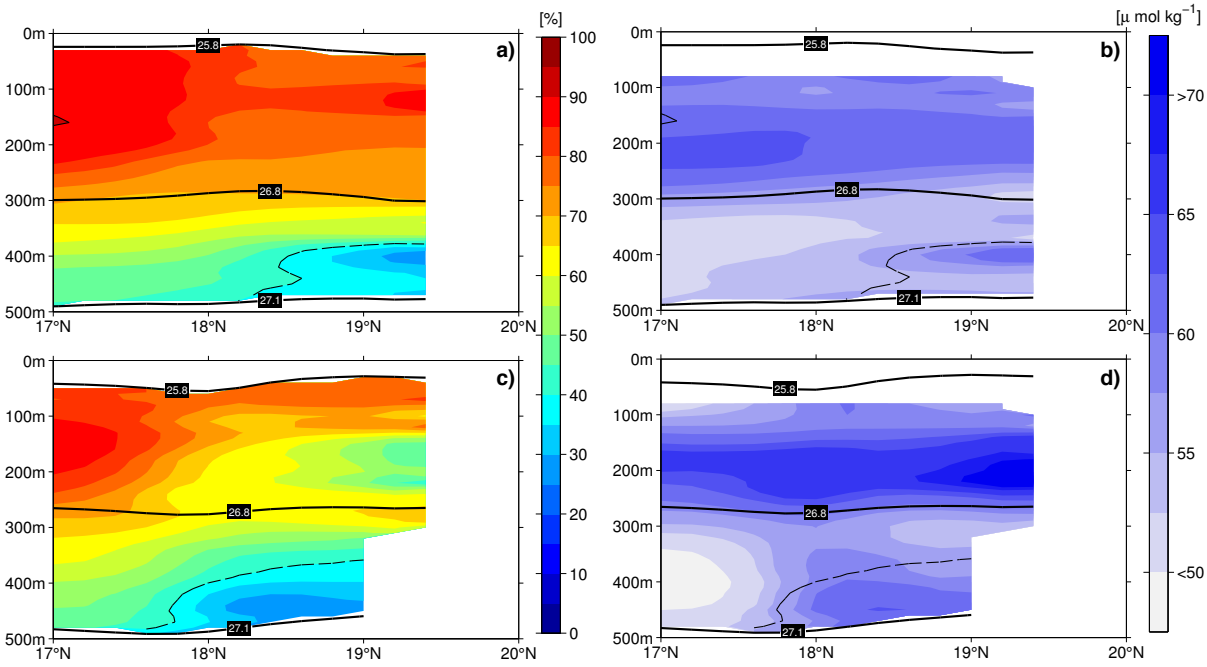

Figure 23: *Same as Figure 22, but for cruise P347. Note that oxygen sampled above water detphs of 90m are excluded.*

In the north/south of the uCW/lCW layers waters consisting mainly of a mixture of SACW and NACW are found, pointing to an older water mass. The difference between the upper and lower central water layers in meridional oxygen distributions becomes clearer when looking at these meridional sections. Generally, oxygen seems to decrease northward in the uCW layer, while in the lCW layer below oxygen decreases southward, due to the influence of NACW from the north. Waters high in central water properties of either hemispheric origin are associated with enhanced oxygen concentrations in both central water layers. This is nicely visible when looking at enhanced oxygen concentrations following the 90%/40% isolines of SACW concentration in the uCW/lCW layers, respectively, during both cruises (Fig.22b,d and Fig.23b,d). The mixture of SACW and NACW that dominates most of the lCW layer along both the off- and near-shore sections during M68/3 exhibits the lowest oxygen concentrations, pointing to an older water mass. The same is true for the very southern end of the lCW layer along both sections during P347.

Oxygen concentrations in the upper layer of the near-shore section during M68/3 are lowest around 100m water depth, decreasing towards the north. The SACW concentration in this oxygen minimum layer is around 80%, lower than water above and below with higher oxygen concentrations. During P347, the shallow minimum is less pronounced but still located around 100m water depth while oxygen concentrations are generally more uniform along the section. The south-north gradient in oxygen concentrations during will likely be carried northward by the boundary current. Overall, oxygen concentrations in the lCW layer during P347 have increased compared to the section recorded during the preceding summer season. This goes along with an overall decrease in SACW concentrations. Judging from the north-south gradient in SACW concentration already apparent during M68/3, this points to an inflow of NACW from the north, carrying higher oxygen waters southward into the lCW.

The relationship between water mass composition and oxygen concentration of a water parcel in the central water stratum is relatively invariant between summer and winter cruises. In general, oxygen concentrations are higher for water parcels of purer NACW/SAWC variety. Water parcels with more or less parts NACW/SACW (SACW content 30%-70%) show lower oxygen concentrations pointing towards an older, not so recently ventilated water mass.

5 Large-Scale Circulation from Sverdrup Dynamics

The circulation on the scale of the tropical gyre in the ETNA is briefly presented using climatological wind stress curl data to calculate the Svertrup transport streamfunction. Note that the presence of the Cape Verde Islands has not been considered when integrating wind stress curl from the eastern boundary. Values for the streamfunction have been assumed to be constant over the islands. Also note that due to the poor data coverage close to the coast, values are likely underestimated. Despite of that, the general structure of the circulation that arises agrees well with the observations presented in the present study as well as with what is generally described in the literature. Further some interesting smaller scale features emerge as well, which will be briefly described here.

The two main large scale circulation features visible in this picture are the two wind-driven gyres. The subtropical gyre is associated with anticyclonic circulation and nega-

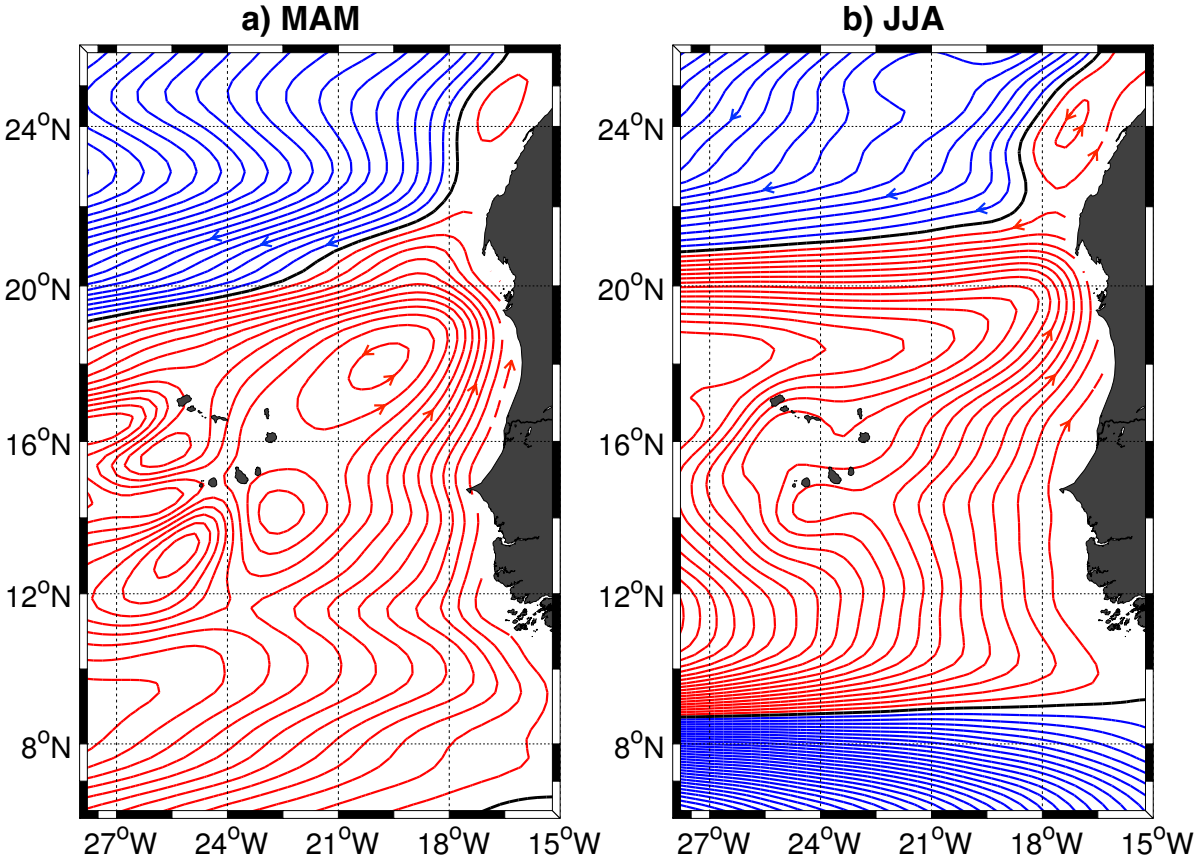

Figure 24: *Transport streamfunction Ψ calculated from SCOW wind stress curl data and integrated westwards from the eastern boundary. Seasonal averages are shown for (a) March, April, May and (b) June, July, August. Streamfunction value intervals are drawn every $0.2Sv$, with red/blue isolines depicting positive/negative values of Ψ. Thick black contour lines mark $\Psi = 0$.*

tive streamfunction values. The region of the subtropical gyre is therefore characterised by subduction. The zero-line of the streamfunction separates it from the tropical gyre to the south. The region of the troipcal gyre is associated with positive Ψ values, cyclonic rotation and hence a region of predominant upwelling (Fig.24). The boundaries of the two gyres vary seasonally, most pronounced at the southern boundary of the tropical gyre. Here eastward flow intensifies during the summer months impinging on the West African coast at around 9°N (Fig.24b). This is likely the seasonal manifestation of the nNECC which is driven by the wind stress curl and is at its maximum during this time due to the northernmost position of the ITCZ. The boundary between the subtropical and tropical gyres in the north varies seasonally, shifting slightly northwards during the summer months. This agrees well with the northward shift of the CC deflection from the African coast during that time. The small scale circulation cells on the lee side of the Cape Verde Islands, most pronounced during March-May, drive localised up- and downwelling.

Prevailing cyclonic wind stress curl along the coast seems to be able to sustain northward flow along the eastern boundary comparable to structure and intensity of the observed currents described ealier. Coming from the south, the streamlines slope northward along the North African coast at around 8°N. The streamfunction reproduces a boundary current of approximately $1.6Sv$ at 18°N on the eastern side of the tropical gyre between 18°- 16°W towards the end of the upwelling season when maximum wind stress curl is observed. Within the coast and 17°W flow is weaker than described before. This could be related to the QuickSCAT data underestimating wind stress curl with respect to ASCAT, as evident from the Sverdrup transport time series presented earlier. Further north the flow recirculates around Cape Blanc between 20°- 22°N and continues southwestward when meeting the anticyclonic circulation of the subtroppical gyre. Part of the eastern boundary flow forms a recirculation gyre-like cell centered around 18°N and 21°W between the coast and the Cape Verde Islands during March-May. The recirculation between 16°-17°N might also be a compensatory response to the divergence in wind stress curl and hence Sverdrup transport at these latitudes This recirculation gyre could act to further distribute SACW in the offshore region or introduce NACW across the CVFZ from the north. Between June-August flow at 18°N is reduced and the recirculation gyre seems to disintegrate.

6 Discussion

In this study the seasonal variability of the boundary circulation in the MUR was investigated using nine research cruises between 2005-2016. Using hydrographic and oxygen data the impact of the seasonal variability of the circulation on the water mass distribution and associated ventilation of the shallow OMZ was analysed. In this section the previously presented results will be discussed. The discussion will mainly focus on two central research questions. First, the renewal of water masses in the central water layer of the MUR through the seasonally varying boundary circulation and secondly, the impact of these water masses on the shallow OMZ. Further, the results of this study will be compared and critically evaluated in the context of previously published studies.

The individual ship sections presented in this study show enhanced northward velocities at 18°N during the relaxation season compared to the upwelling season. Strongest currents are confined to the surface layer as well as the upper uCW layer and extend over the entire continental shelf. These conditions reflect a shoaling or possibly an outcropping of the PUC in combination with an intensified surface MC, coinciding with seasonally intensified nNECC transport in the south (*Stramma et al.* [2005]) as well as the rapid warming of near-coastal SSTs in the region to about 20°N (e.g. *Lathuilière et al.* [2008]). The general shape, structure and speeds of the observed currents agree well with previous descriptions by e.g. *Mittelstaedt* [1983] and *Peña-Izquierdo et al.* [2012]. The intensification of northward transports in the uCW layer follows the seasonal cycle of wind stress curl at these latitudes. As previously shown by e.g. *McCreary Jr. et al.* [1987] and *Marchesiello et al.* [2003] for the California Current system, the PUC is a direct response to cyclonic wind stress curl inducing poleward Sverdrup transport. *Marchesiello et al.* [2003] were able to directly compare upper ocean transports in their model to Sverdrup transport from reanalysis wind stress curl data and found them to be in good agreement. Sverdrup transport calculated in this study is able to account for a large part of the variability observed in the ship sections and the calculated transports agree quite well. However, other processes driving northward velocities could lead to deviations from Sverdrup dynamics. *Mittelstaedt* [1983] reported that a meridional pressure gradient along the coast is caused by the deviation of the CC from the coast at mid-latitudes and an excess of water masses at the eastern margin of the tropical Atlantic due to the NECC and NEUC. This barotropic pressure gradient leads to compensatory flow over the shelf that is expected to be strongest in summer, but masked by southward flow over the shelf when meridional wind stress is at its peak. Additionally, *Marchesiello et al.* [2003] showed for the California Current Region that eddies could act to enhance or decrease boundary current transport. Strong mesoscale activity is a large driver of variability in the MUR

as well (e.g. *Schütte et al.* [2016]), to be discussed further later on in this section.

Penven et al. [2005] attributed the shallow core as well as the occasional outcropping of the Peru-Chile Undercurrent in the Peruvian Current System to the strong cyclonic wind stress curl close to the coast. Wind stress curl in the MUR is also strongly cyclonic in a band roughly 200km from the coast during early boreal summer, possibly leading to the shoaling and surface intensification of the PUC observed during several cruises in this study. The Sverdrup streamfunction calculated from climatological wind stress curl data between 1999-2009 supports the existence of a seasonally intensified PUC along the Mauritanian coast. The streamfunction also reproduces a recirculation gyre south of Cape Blanc between the Cape Verde Islands and the coast. The recirculation gyre has been previously proposed by *Mittelstaedt* [1983] to be formed in part by extensions of the CC, or by *Peña-Izquierdo et al.* [2012] to explain regional distributions of low oxygen concentrations. It is most defined between March-May, when cyclonic wind stress curl close to the coast around Cape Blanc is at its seasonal maximum and wind stress curl offshore is negative. The ocean circulation in the upper 50-200m in the ETNA emerging from a ten year-average of Simple Ocean Data Assimilation model output described by *Stramma et al.* [2016] displays a similar feature in the same region. The recirculation gyre, albeit weaker, reappears during October/November (not shown), agreeing with the observed semiannual cycle in wind stress curl observed in satellite data around these latitudes. *Peña-Izquierdo et al.* [2012] reported enhanced northward transports in the uCW layer along the coast. Their results are based on observations during a single cruise in November 2008. The shape and magnitude of the observations during periods of enhanced wind stress curl described in this present study match theirs. Also the enhanced northward transport fits the seasonality of the wind stress curl that is apparent in the satellite data and strengthens our confidence in the results presented during this study. It also serves to supplement our results which lack observations from the end of summer until the early winter months. However, their conclusion that the observed currents and oxygen concentrations represent typical late summer/early autumn conditions is not necessarily true. Due to the semi-annual cycle in the wind stress curl conditions during their cruise might very well be representative typical late autumn/early winter conditions and provide further evidence for ventilation through SACW in the uCW layer in the second half of the year.

The mean circulation during the upwelling season exhibits less intense northward flow attached to the slope and shelf break between about 100-200m depth. Over the continental shelf southward flow is present in most of the winter sections as a geostrophic response to coastal upwelling. This equatorward jet has previously been described by e.g. *Mit-*

telstaedt [1983] and shifts the countercurrent away from the coast during the upwelling season (*Barton* [1989]). The mean meridional velocity section during the upwelling season resembles model simulations of the geostrophic response of the coastal circulation forced by positive wind stress curl performed by *McCreary and Chao* [1985]. The equatorward jet displacing the poleward undercurrent over the shelf was also observed by *Penven et al.* [2005] over the Peruvian shelf.

Northward velocities close to the slope and shelf break during both seasons are confined to the uCW layer while in the lCW layer below velocities are predominantly southward. We observe southward velocities of smaller magnitude compared to the northward velocities in the uCW layer in almost all our ship sections. The seasonality in this lower layer is comparable to that observed in the upper layer, southward flow intensifies during the relaxation season. The observed circulations in the two central water layers resemble the near-shore limbs of two opposing circulation cells in the upper and lower central water layers proposed by *Peña-Izquierdo et al.* [2015] on the basis of model experiments and *Peña-Izquierdo et al.* [2012] through observations. As mentioned previously, poleward flow in the uCW water layer is to a large extent forced directly by seasonally intensified cyclonic wind stress curl. The exact physical forcing mechanism leading to opposed circulation in the layer beyond is beyond the scope of this study. However, as shown in the meridional water mass property sections, and previously discussed by *Peña-Izquierdo et al.* [2015], the layer thicknesses of upper and lower central water layers covary and a thickening of the uCW induces a thinning of the lCW layer. Southward velocities could be a means of potential vorticity conservation in response to vortex squashing.

In agreement with the observed current conditions, the highest SACW concentrations in the boundary region around 18°N are observed during the relaxation season. We observed a freshening and cooling in the uCW layer throughout our summer cruises, most evident in the relaxation season mean. This implies that the main renewal of upper central water layers in the MUR occurs mainly during early summer, when upwelling-favorable winds are weak and the surface MC and subsurface PUC transport fresh SACW northward along the boundary. It could further be shown that seasonally SACW can dominate the uCW layer in the boundary current regime 100km from the coast as far north as 20°N as a result of intensified northward transport inside the PUC and MC and associated advection of southern waters. Highest concentrations of SACW are found in the boundary current region, while in the region of the recirculation gyre lower SACW concentrations point to a mixed water mass. The presence of high SACW concentrations in the uCW layer further from the coast south of 18°N suggests that this particular region of the MUR is filled with SACW supplied by the nNECC during early summer.

Using the water mass analysis method described by *Johns et al.* [2003], it could be shown that the change in central water characteristics from predominantly SACW in the uCW layer to a mixture of SACW and NACW in the lCW layer is a consistent property of the central water stratum in the region and was observed throughout all cruises presented in this study. The change occurs around the $26.8 kgm^{-3}$-isopycnal and coincides with the opposing circulations observed in these layers, suggesting a change in source water for the ventilation and renewal of water masses in the respective layers. This has been previously proposed through modelling studies by *Elmoussaoui et al.* [2005] or *Peña-Izquierdo et al.* [2015] and through observed hydrographic properties and oxygen distribution by *Voituriez and Chuchla* [1978]. On the basis of their observations, which lacked southward velocities in the lCW layer, *Peña-Izquierdo et al.* [2012] suggested this circulation to be intermittent and likely seasonal. In our data set during P320 no southward velocities in the lCW were observed, however water mass concentrations still point to a mixture of the two central water masses and even show enhanced NACW concentrations. The exact contribution of southern central waters certainly depends on the definition of *typical* SACW properties used for the water mass analysis, but calculated SACW concentrations in the two layers agree well with the ones described by *Peña-Izquierdo et al.* [2015] from observational data as well as model output.

The observed regime change is likely connected to the vertical extent of the eastward flowing NEUC and NECC transporting southern waters eastward. Using lowered ADCP measurements along 35°W, *Schott et al.* [2003] found the lower boundary of the NEUC to be at around the $26.8 kgm^{-3}$-isopycnal. This was validated and shown for the NECC as well by *Elmoussaoui et al.* [2005] through model experiments. These currents therefore supply the water to renew the uCW layer. Our observations during at least two cruises further directly show the advection of NACW from the north in the lCW layer. Even though southward currents in the lCW layer are more pronounced during the summer months, the percentage of NACW in that layer is higher in winter. This could also have implications for the ventilation of the deep oxygen minimum layers, as already proposed by *Voituriez and Chuchla* [1978].

Meridional sections of water mass properties and oxygen concentrations showed that waters high in SACW advected from the south as well as NACW coming from the north are higher in oxygen concentrations with respect to the ambient waters. *Pastor et al.* [2012] also showed that water masses exhibiting NACW characteristics are associated with higher oxygen concentrations, due to their more recent ventilation and subduction in the subtropical gyre to the north of the study region. The mixture of SACW and NACW waters found mostly in the southern lCW and northern uCW layers, previously

identified as a regional water mass and termed the Cape Verde SACW (SACWcv) by *Peña-Izquierdo et al.* [2012], is a signature of an older, not recently replenished water mass as is evident when looking at associated oxygen concentrations. Oxygen concentrations associated with this CW-variety are lower than those observed in water masses high in SACW or NACW concentrations due to a longer residence time and oxygen consumption through remineralisation.

The oxygen decrease from the uCW to the lCW that is apparent throughout all cruises has previously been reported by e.g. *Peña-Izquierdo et al.* [2015] and agrees well with our observations of water mass and circulation changes between those layers. Variability in this layer is associated with NACW intrusions from the north and the west and was most pronounced during two winter cruises. The renewal of water masses in the uCW layer through the seasonally intensified boundary currents should manifest itself in higher oxygen concentrations at the shelf break in the region of the shallow oxygen minimum. However, despite the advection of purer SACW in the uCW particularly during the relaxation season, very low oxygen concentrations close to the shelf break as well as extending laterally offshore at 18°N are observed during two summer cruises. The offshore minimum right around 100m water depth and just below the $26.3 kgm^{-3}$-isopycnal in the region of the recirculation gyre was especially pronounced during M129, with oxygen concentrations below $40 \mu molkg^{-1}$ throughout the region.

It could be shown that chlorophyll concentrations in the surface layer between 17°-19°N remain high and extend up to 600km offshore for 1-2 months after upwelling-favorable winds along the coast have seized, as previously described by *Lathuilière et al.* [2008]. They further reported nutrient limitation to be important in determining the amount and limiting the growth of cholorophyll in the surface layer, but ruled it out as a regulating factor in the MUR. As could be shown in this study, the upwelled waters in the MUR are central waters of predominantly South Atlantic origin. Due to the high nutrient content of these waters relative to the NACW (e.g. *Pastor et al.* [2012]) nutrient limitation is likely not a factor for the upwelled waters in the MUR and nutrients are advected offshore by Ekman transport before being used up by biology (*Lathuilière et al.* [2008]). Recently, *Gruber et al.* [2011] have analysed the effect of eddies on the near- and offshore primary production in eastern boundary upwelling systems, with a particular focus on the California and Canary Upwelling Systems. They found that eddies tend to reduce production in nearshore regimes, while enhancing it in offshore regions through lateral transport of nutrients in the euphotic layer. This excess of nutrients can sustain phytoplancton growth into the relaxation season, when alongshore winds are already decreasing and rapid restratification occurs. This was also discussed by *Brink* [1983] as a mechanism

to prolong biological productivity. It is this prolonged phytoplancton growth, which in turn extends the period of remineralization, together with the rapid restratification and a shoaling oxycline at the beginning of the relaxation season that could be a reason for the low oxygen concentrations observed offshore during the summer cruises particularly during M107 and M129, and in the northern part of the study region during M68/3.

Minimum oxygen concentrations at the shelf break during the summer months could be related to a weaker influence of diapycnal oxygen fluxes at depths above 300m water depth during that season. Diapycnal oxygen fluxes above 500m water depth during two winter cruises were reported to be between 44 and 105 $mmolm^{-2}d^{-1}$ (*Schafstall et al.* [2010]), exceeding the benthic oxygen uptake by a factor of about 7 (*Brandt et al.* [2015]). Due to stronger stratification over the continental slope and shelf however, the diapycnal supply of oxygen from the surface into the stratified ocean would be greatly reduced during summer months, even assuming dissipation rates during summer remaining similar to those reported by *Schafstall et al.* [2010]. Benthic oxygen uptake was found to exhibit almost no seasonal variability by *Dale et al.* [2014], and be as high as $10mmolm^{-2}d^{-1}$ for water depths between 50-100m, which coincides with regions of extremely low oxygen concentrations during M107 and M129. In the absence of diapycnal oxygen supply from the well-ventilated surface layer and isopycnal supply as evident during the upwelling season, these fluxes could potentially lead to low oxygen concentrations during periods of variable boundary circulation.

One important aspect that has not been explicitly discussed so far is the high variability that is apparent in the cruise data on timescales of days to weeks. Especially pronounced during cruises P347 and M107, where sections were profiled several times within a couple of weeks, the undercurrent exhibited strong variability. This variability could point to a meandering of the undercurrent or be related to variability in wind forcing. *Mittelstaedt* [1983] reported that the wind stress varies on timescales of five to ten days. Similarly, *Lathuilière et al.* [2008] were able to attribute intense, intermittent periods of phytoplancton growth to short-term variations of along-shore wind stress. Variability on these short timescales is apparent in the Sverdrup transport time series presented earlier as well. The response of the boundary circulation to wind stress curl changes should be fairly rapid (e.g. *Elmoussaoui et al.* [2005]) due to the close vicinity to the eastern boundary. This variability is apparent during both summer and winter cruises and could be associated with variability in wind forcing.

Due to the enhanced and pronounced mesoscale eddy activity in the MUR especially during early summer (*Schütte et al.* [2016]), individual ship sections as well as mean seasonal sections are not free of the effect of eddies. The period of maximum eddy

generation proposed by *Schütte et al.* [2016] coincides with the period of rapid decrease in Sverdrup transport. During this time the boundary current weakens as well, as seen during cruise M129, when negligible northward transport in the uCW layer during a period of weak (close to zero) Sverdrup transport was observed. Due to the sudden decrease in vorticity input by cyclonic wind stress curl that seems to be a consistent seasonal feature in the time series presented earlier, the PUC may disintegrate into eddies to conserve its vorticity, which then transport coastal waters of mainly South Atlantic origin into the open ocean. Some of these eddies were found to carry with them in their core waters of extremely low oxygen concentrations (*Karstensen et al.* [2015]). An Anticyclonic mode water eddy exhibiting extremely low oxygen concentrations (less than $10 \mu mol kg^{-1}$) just below the surface layer was observed not far from the coast during M129. Assuming a westward propagation speed of $3 \pm 2.5 km d^{-1}$ (*Schütte et al.* [2016]), the eddy could have been generated a minimum of 40 days prior to its detection during a period of vigorous decrease in wind stress curl and hence Sverdrup transport. The already low oxygen concentrations at the shelf break observed during that cruise might explain the extreme oxygen minimum observed inside the eddy, while the low oxygen concentrations at the shelf break during the summer months suggest an impact on the processes and the nature of these eddies in general.

7 Conclusion and Outlook

Based on the observations presented in this study the seasonality of the boundary circulation in the coastal upwelling region of the ETNA can be summarised as follows: During the upwelling season we find equatorward flow over the shelf as a direct geostrophic response to lower sea level close to the coast forced by offshore Ekman transport through peak southward wind stress. The undercurrent during this time is confined to a core of northward velocities of around 100m depth and 30-40km width. Velocities do not exceed far beyond $10 cm s^{-1}$. Once upwelling favorable wind stress dies down a countercurrent develops over the shelf that transports warm water from the south into the near-shore region leading to a rapid restratification and rapid decrease in surface chlorophyll concentrations. The poleward undercurrent strengthens and shifts vertically as a direct response to enhanced Sverdrup transport forced by cyclonic wind stress curl, confining strongest current velocities to the surface and upper uCW layers. This strengthening seizes once Sverdrup transport drops rapidly and the relaxation season comes to an end in August-September. The renewal of water masses through the advection of SACW in the boundary currents occurrs mainly in the uCW layer during the relaxation season, suggested by the observed large amounts of waters high in SACW charactersitics during that season. This seasonal variability attributed to the impact of the strengthened boundary currents can be traced as far north as 20°N, and probably further, but lacking sufficient observations there.

The observations made in this study suggest that a shallow oxygen minimum exists at the shelf break despite seasonal renewal of uCW layers and the supply of SACW. Prolonged remineralisation in the wake of the upwelling season in combination with absent diapycnal fluxes from the surface layer inhibited by strong and rapid restratification are identified as the possible cause. The offshore oxygen minimum around 100m water depth forms after upwelling-favorable winds have seized and persists afterwards due to prolonged productivity in the surface layer and associated oxygen consumption below. The prolonged productivity in that region stems from nutrient-rich waters advected offshore by eddies and Ekman transport. Boundary currents do not reach this region of the MUR, which is further characterised by a cyclonic circulation cell and older water masses. The deep oxygen minimum, situated at the lower end of the lCW stratum and associated with weak southward velocities and older water masses, is caused by weak ventilation in combination with oxygen consumption that, albeit low, due to the long residence time leads to the observed low oxygen concentrations.

To better analyse the dependence of the boundary circulation on the wind forcing and understand the response of the PUC to seasonal and short-term variability in particular, moored observations of velocities and hydrography over the continental slope and shelf for at least one year would be of great value. Further, the complex biogeochemical and physcial/dynamical processes that determine the structure of the shallow OMZ close to the eastern boundary need to be further investigated.

However, based on the transport estimates from shipboard current measurements and hydrographic conditions observed during the several cruises and analysed in this study, the general picture that arises is in good agreement with observational and modeling efforts performed in the past.

References

Albert, A., V. Echevin, M. Lévy, and O. Aumont (2010), Impact of nearshore wind stress curl on coastal circulation and primary productivity in the Peru upwelling system, *Journal of Geophysical Research: Oceans*, *115*(12), 1–13, doi:10.1029/2010JC006569.

Banyte, D., T. Tanhua, M. Visbeck, D. W. R. Wallace, J. Karstensen, G. Krahmann, A. Schneider, L. Stramma, and M. Dengler (2012), Diapycnal diffusivity at the upper boundary of the tropical North Atlantic oxygen minimum zone, *Journal of Geophysical Research*, *117*, 1–14, doi:10.1029/2011JC007762.

Barton, E. (1989), The poleward undercurrent on the eastern boundary of the subtropical North Atlantic., in *Poleward Flows Along Eastern Boundaries*, vol. 34, pp. 82–95, Springer New York.

Barton, E. D., et al. (1998), The transition zone of the Canary Current upwelling region, *Progress in Oceanography*, *41*(4), 455–504, doi:10.1016/S0079-6611(98)00023-8.

Brandt, P., V. Hormann, A. Körtzinger, M. Visbeck, G. Krahmann, L. Stramma, R. Lumpkin, and C. Schmid (2010), Changes in the Ventilation of the Oxygen Minimum Zone of the Tropical North Atlantic, *Journal of Physical Oceanography*, *40*(8), 1784–1801, doi:10.1175/2010JPO4301.1.

Brandt, P., et al. (2015), On the role of circulation and mixing in the ventilation of oxygen minimum zones with a focus on the eastern tropical North Atlantic, *Biogeosciences*, *12*(2), 489–512, doi:10.5194/bg-12-489-2015.

Brink, K. (1983), The near-surface dynamics of coastal upwelling, *Progress in Oceanography*, *12*(3), 223–257, doi:10.1016/0079-6611(83)90009-5.

Brink, K., D. Halpern, A. Huyer, and R. Smith (1983), The Physical Environment of the Peruvian Upwelling System, *Progress in Oceanography*, *12*, 285–305.

Capet, X. J., P. Marchesiello, and J. C. McWilliams (2004), Upwelling response to coastal wind profiles, *Geophysical Research Letters*, *31*(13), 1–4, doi:10.1029/2004GL020123.

Chaigneau, A., N. Dominguez, G. Eldin, L. Vasquez, R. Flores, C. Grados, and V. Echevin (2013), Near-coastal circulation in the Northern Humboldt Current System from shipboard ADCP data, *Journal of Geophysical Research: Oceans*, *118*(10), 5251–5266, doi:10.1002/jgrc.20328.

Dale, A. W., S. Sommer, E. Ryabenko, A. Noffke, L. Bohlen, K. Wallmann, K. Stolpovsky, J. Greinert, and O. Pfannkuche (2014), Benthic nitrogen fluxes and fractionation of nitrate in the Mauritanian oxygen minimum zone (Eastern Tropical North Atlantic), *Geochimica et Cosmochimica Acta*, *134*, 234–256, doi:10.1016/j.gca.2014.02.026.

Echevin, V., F. Colas, A. Chaigneau, and P. Penven (2011), Sensitivity of the Northern Humboldt Current System nearshore modeled circulation to initial and boundary conditions, *Journal of Geophysical Research: Oceans*, *116*(7), 1–16, doi:10.1029/2010JC006684.

Echevin, V., A. Albert, M. Lévy, M. Graco, O. Aumont, A. Piétri, and G. Garric (2014), Intraseasonal variability of nearshore productivity in the Northern Humboldt Current System: The role of coastal trapped waves, *Continental Shelf Researchn*, *73*(January 2013), 14–30, doi:10.1016/j.csr.2013.11.015.

Ekau, W., H. Auel, H.-O. Pörtner, and D. Gilbert (2010), Impacts of hypoxia on the structure and processes in pelagic communities (zooplankton, macro-invertebrates and fish), *Biogeosciences*, pp. 1669–1699, doi:10.5194/bg-7-1669-2010.

Elmoussaoui, A., M. Arhan, and A. M. Treguier (2005), Model-inferred upper ocean circulation in the eastern tropics of the North Atlantic, *Deep-Sea Research Part I: Oceanographic Research Papers*, *52*(7), 1093–1120, doi:10.1016/j.dsr.2005.01.010.

Fennel, W. (1999), Theory of the Benguela Upwelling System, *Journal of Physical Oceanography*, *29*(2), 177–190, doi:10.1175/1520-0485(1999)029¡0177:TOTBUS¿2.0.CO;2.

Fischer, T., D. Banyte, P. Brandt, M. Dengler, G. Krahmann, T. Tanhua, and M. Visbeck (2013), Diapycnal oxygen supply to the tropical North Atlantic oxygen minimum zone, *Biogeosciences*, *10*(7), 5079–5093, doi:10.5194/bg-10-5079-2013.

Glessmer, M. S., C. Eden, and A. Oschlies (2009), Contribution of oxygen minimum zone waters to the coastal upwelling off Mauritania, *Progress in Oceanography*, *83*(1-4), 143–150, doi:10.1016/j.pocean.2009.07.015.

Gruber, N., Z. Lachkar, H. Frenzel, P. Marchesiello, M. Münnich, J. C. McWilliams, T. Nagai, and G.-K. Plattner (2011), Eddy-induced reduction of biological production in eastern boundary upwelling systems, *Nature Geoscience*, *4*(11), 787–792, doi:10.1038/ngeo1273.

Johns, W. E., R. J. Zantopp, and G. J. Goni (2003), Cross-gyre transport by North Brazil Current rings, *Elsevier Oceanogr. Serie.*, *68*, 411–441.

Karstensen, J., L. Stramma, and M. Visbeck (2008), Oxygen minimum zones in the eastern tropical Atlantic and Pacific oceans, *Progress in Oceanography*, *77*(4), 331–350, doi:10.1016/j.pocean.2007.05.009.

Karstensen, J., et al. (2015), Open ocean dead zones in the tropical North Atlantic Ocean, *Biogeosciences*, *12*, 2597–2605, doi:10.5194/bg-12-2597-2015.

Kirchner, K., M. Rhein, S. Hüttl-Kabus, and C. W. Böning (2009), On the spreading of South Atlantic Water into the Northern Hemisphere, *Journal of Geophysical Research*, *114*, C05,019, doi:10.1029/2008JC005165.

Large, W. G., and S. Pond (1981), Open Ocean Momentum Flux Measurements in Moderate to Strong Winds, doi:10.1175/1520-0485(1981)011¡0324:OOMFMI¿2.0.CO;2.

Lathuilière, C., V. Echevin, and M. Lévy (2008), Seasonal and intraseasonal surface chlorophyll-a variability along the northwest African coast, *Journal of Geophysical Research*, *113*, 2000–2004, doi:10.1029/2007JC004433.

Luyten, J., J. Pedlosky, and H. Stommel (1983), The ventilated thermocline, doi:10.1175/1520-0485(1983)013¡0292:TVT¿2.0.CO;2.

Marchesiello, P., J. C. McWilliams, A. Shchepetkin, P. Physics, and L. Angeles (2003), Equilibrium Structure and Dynamics of the California Current System, *Journal of Physical Oceanography*, *33*(4), 753–783, doi:10.1175/1520-0485(2003)33¡753:ESADOT¿2.0.CO;2.

McCreary, J. P., and S.-Y. Chao (1985), Three-dimensional shelf circulation along an eastern ocean boundary, *Journal of Marine Research*, *43*(1), 13–36, doi:doi:10.1357/002224085788437316.

McCreary Jr., J. P., P. K. Kundu, and S.-Y. Chao (1987), On the dynamics of the California Current system, *Journal of Marine Research*, *45*(1).

Mittelstaedt, E. (1976), On the Currents along the Northwest African Coast South of 22° North, *Deutsche Hydrographische Zeitschrift*, *29*(3).

Mittelstaedt, E. (1983), The upwelling area off Northwest Africa-A description of phenomena related to coastal upwelling, *Progress in Oceanography*, *12*(3), 307–331, doi:10.1016/0079-6611(83)90012-5.

Mittelstaedt, E. (1991), The ocean boundary along the northwest African coast: Circulaton and oceanographic properties at the sea surface, *Progressive Oceanography*, *26*.

Nykjaer, L., and L. Van Camp (1994), Seasonal and interannual variability of coastal upwelling along northwest Africa and Portugal from 1981 to 1991, *Journal of Geophysical Research*, *99*, 14,197–14,207.

Pastor, M. V., J. Peña-Izquierdo, J. L. Pelegrí, and Á. Marrero-Díaz (2012), Meridional changes in water mass distributions off NW Africa during November 2007/2008, *Ciencias Marinas*, *38*, 223–244.

Peña-Izquierdo, J., J. L. Pelegrí, M. V. Pastor, P. Castellanos, M. Emelianov, M. Gasser, J. Salvador, and E. Vázquez-Domínguez (2012), The continental slope current system between Cape Verde and the Canary Islands, *Scientia Marina*, *76*(S1), 65–78, doi: 10.3989/scimar.03607.18C.

Peña-Izquierdo, J., E. Van Sebille, J. Pelegri, J. Sprintall, E. Mason, P. Llanillo, and F. Machin (2015), Water mass pathways to the North Atlantic oxygen minimum zone, *Journal of Geophysical Research : Oceans*, (120), 3350–3372, doi: 10.1002/2014JC010557.Received.

Penven, P., V. Echevin, J. Pasapera, F. Colas, and J. Tam (2005), Average circulation, seasonal cycle, and mesoscale dynamics of the Peru Current System: A modeling approach, *Journal of Geophysical Research C: Oceans*, *110*(10), 1–21, doi: 10.1029/2005JC002945.

Polo, I., A. Lazar, B. Rodriguez-Fonseca, and S. Arnault (2008), Oceanic Kelvin waves and tropical Atlantic intraseasonal variability: 1. Kelvin wave characterization, *Journal of Geophysical Research: Oceans*, *113*(7), 1–18, doi:10.1029/2007JC004495.

Reid, J. L. (1994), On the total geostrophic circulation of the North Atlantic Ocean: Flow patterns, tracers, and transports, *Progress in Oceanography*, *33*, 1–92.

Rhein, M., K. Kirchner, C. Mertens, R. Steinfeldt, M. Walter, and U. Fleischmann-wischnath (2005), Transport of South Atlantic water through the passages south of Guadeloupe and across 16°N, 2000–2004, *Deep Sea Research Part I: Oceanographic Research Papers*, *52*, 2234–2249, doi:10.1016/j.dsr.2005.08.003.

Risien, C. M., and D. B. Chelton (2008), A Global Climatology of Surface Wind and Wind Stress Fields from Eight Years of QuikSCAT Scatterometer Data, *Journal of Physical Oceanography*, *38*(11), 2379–2413, doi:10.1175/2008JPO3881.1.

Schafstall, J. (2010), Turbulente Vermischungsprozesse und Zirkulation im Auftriebsgebiet vor Nordwestafrika, Ph.D. thesis, Kiel University.

Schafstall, J., M. Dengler, P. Brandt, and H. Bange (2010), Tidal-induced mixing and

diapycnal nutrient fluxes in the Mauritanian upwelling region, *Journal of Geophysical Research*, *115*(C10), C10,014, doi:10.1029/2009JC005940.

Schmidtko, S., G. C. Johnson, and J. M. Lyman (2013), MIMOC: A global monthly isopycnal upper-ocean climatology with mixed layers, *Journal of Geophysical Research: Oceans*, *118*(4), 1658–1672, doi:10.1002/jgrc.20122.

Schott, F. A., M. Dengler, P. Brandt, K. Affler, J. Fischer, B. Bourlès, Y. Gouriou, R. L. Molinari, and M. Rhein (2003), The zonal currents and transports at 35°W in the tropical Atlantic, *Geophysical Research Letters*, *30*(7), 1349, doi:10.1029/2002GL016849.

Schütte, F., P. Brandt, and J. Karstensen (2016), Occurrence and characteristics of mesoscale eddies in the tropical northeastern Atlantic Ocean, *Ocean Science*, *12*, 663–685, doi:10.5194/os-12-663-2016.

Stramma, L., S. Hüttl, and J. Schafstall (2005), Water masses and currents in the upper tropical northeast Atlantic off northwest Africa, *Journal of Geophysical Research: Oceans*, *110*(12), 1–18, doi:10.1029/2005JC002939.

Stramma, L., P. Brandt, J. Schafstall, F. Schott, J. Fischer, and A. Körtzinger (2008a), Oxygen minimum zone in the North Atlantic south and east of the Cape Verde Islands, *Journal of Geophysical Research: Oceans*, *113*(4), 1–15, doi:10.1029/2007JC004369.

Stramma, L., G. C. Johnson, J. Sprintall, and V. Mohrholz (2008b), Expanding Oxygen-Minimum Zones in the Tropical Oceans, *Science (New York, N.Y.)*, *2006*(May), 2006–2009, doi:10.1126/science.1153847.

Stramma, L., R. Czeschel, T. Tanhua, P. Brandt, M. Visbeck, and B. S. Giese (2016), The flow field of the upper hypoxic eastern tropical North Atlantic oxygen minimum zone, *Ocean Science*, *12*, 153–167, doi:10.5194/os-12-153-2016.

Sverdrup, H. U. (1947), Wind-driven currents in a baroclinic ocean; with application to the equatorial currents of the eastern Pacific, *Proc. Natl. Acad. Sci.*, (1), 318–326.

Tomczak, M. (1981), An analysis of mixing in the frontal zone of South and North Atlantic Central Water off North-West Africa, *Progress in Oceanography*, *10*, 173–192.

Van Camp, L., L. Nykjaer, E. Mittelstaedt, and P. Schlittenhardt (1991), Upwelling and boundary circulation off Northwest Africa as depicted by infrared and visible satellite observations, *Progress in Oceanography*, *26*, 357–02.

Voituriez, B., and R. Chuchla (1978), Influence of the Southern Atlantic Central Water on the distribution of salinity and oxygen in the northeast tropical Atlantic Ocean, *Deep-Sea Research*, *25*, 107–117.

Wyrtki, K. (1962), The oxygen minima in relation to ocean circulation, *Deep Sea Research and Oceanographic Abstracts*, *9*, 11–23, doi:10.1016/0011-7471(62)90243-7.

Zenk, W., B. Klein, and M. Schroder (1991), Cape Verde Frontal Zone, *Deep Sea Research Part A, Oceanographic Research Papers*, *38*, 505–530, doi:10.1016/S0198-0149(12)80022-7.

Acknowledgements

I want to thank Peter Brandt and Marcus Dengler for providing me with the topic for this thesis, giving me the opportunity to collect some of my data on research cruise M129 as well as their supervision throughout the last six months. I'd further like to thank all the captains and crew of the research vessels *Poseidon, Meteor, L'Atalante* and *Maria S. Merian*, as well as all scientists involved in the various research cruises. A big thank you also goes to Sunke Schmidtko for providing me with data from the MIMOC climatology.

Thanks to Florian Schütte for fruitful discussions and making data collection from the various cruises that much easier. Special thanks are due to Robert Kopte and Franz Philip Tuchen for all the less fruitful discussions that kept me sane and motivated.

Erklärung

Hiermit erkläre ich, dass ich die vorliegende Arbeit selbständig und ohne fremde Hilfe angefertigt und keine anderen als die angegebenen Quellen und Hilfsmittel verwendet habe.

Die eingereichte schriftliche Fassung der Arbeit entspricht der auf dem elektronischen Speichermedium (benannt mit *1005607.pdf*). Weiterhin versichere ich, dass diese Arbeit noch nicht als Abschlussarbeit an anderer Stelle vorgelegen hat.

Thilo Klenz, Dezember 2016